Tectonophysics 474 (2009) 526–543

Contents lists available at ScienceDirect

Tectonophysics

journal homepage: www.elsevier.com/locate/tecto

Flexural isostasy in the Bolivian Andes: Chaco foreland basin development

Claudia B. Prezzi [a,*], Cornelius E. Uba [b], Hans-Jürgen Götze [c]

[a] CONICET, Universidad de Buenos Aires, INGEODAV, Dpto. de Cs. Geológicas, FCEyN, Universidad de Buenos Aires, Ciudad Universitaria, Pabellón 2, 1428, Buenos Aires, Argentina
[b] Institut für Geowissenschaften, Universität Potsdam, Karl-Liebknecht-Str 25, 14476 Potsdam, Germany
[c] Institut für Geowissenschaften, Abteilung Geophysik, Christian Albrechts Universität, Otto-Hahn-Platz 1, 24118 Kiel, Germany

ARTICLE INFO

Article history:
Received 29 July 2008
Received in revised form 13 March 2009
Accepted 28 April 2009
Available online 5 May 2009

Keywords:
Central Andes
Chaco foreland
Flexural isostasy
Flexural modelling
Basin development

ABSTRACT

The Chaco foreland basin was initiated during the late Oligocene as a result of thrusting in the Eastern Cordillera in response to Nazca–South America plate convergence. Foreland basins are the result of the flexural isostatic response of an elastic plate to orogenic and/or thrust sheet loading. We carried out flexural modelling along a W–E profile (21.4°S) to investigate Chaco foreland basin development using new information on ages of foreland basin strata, elastic and sedimentary thicknesses and structural histories. It was possible to reproduce present-day elevation, gravity anomaly, Moho depth, elastic thicknesses, foreland sedimentary thicknesses and the basin geometry. Our model predicted the basin geometry and sedimentary thicknesses for different evolutionary stages. Measured thicknesses and previously proposed depozones were compared with our predictions. Our results shed more light on the Chaco foreland basin evolution and suggest that an apparent decrease in elastic thickness beneath the Eastern Cordillera and the Interandean Zone could have occurred between 14 and 6 Ma.

1. Introduction

Foreland basins form as a result of the migration of thrust belts, and are modified by processes such as crustal thickening, mass transport by erosion–sedimentation and regional isostatic subsidence (e.g., Jordan and Flemings, 1991; DeCelles and Giles, 1996; Catuneanu, 2004). Therefore, foreland basins are the result of the flexural isostatic response of an elastic plate to orogenic and/or thrust sheet loading (Beaumont, 1981; Jordan, 1981; DeCelles and Giles, 1996). These basins are characterized by elongated troughs parallel to the associated loads, showing asymmetrical geometry, with the sediment-fill thickening to the zone adjacent to the thrust load (Beaumont, 1981; DeCelles and Giles, 1996). The evolution of the associated orogen and the rheological state of the lithosphere are recorded by the architecture of the different stratigraphic units (derived from the sediments supplied by the eroding mountain belt) that constitute the infill of the foreland basin (e.g., Beaumont, 1981; Flemings and Jordan, 1989). DeCelles and Giles (1996) characterized foreland basin systems into four depozones starting from the proximal part with the thrust load, wedge-top through foredeep and forebulge, finally to the backbulge close to the craton.

The Chaco foreland basin developed in response to the fold and thrust belt evolution in the backarc region of the Central Andes (Fig. 1). The basin is a classic example of a foreland basin system in a backarc position. Detailed structural studies have resulted in construction of balanced cross-sections (e.g., Kley et al., 1996; McQuarrie, 2002) and documentation of the timing and amount of shortening (e.g., Kley et al., 1997; McQuarrie et al., 2005; Ege et al., 2007). Additionally, thermal models (Springer, 1999) and elastic thickness calculations (Tassara, 2005; Tassara et al., 2006) helped define both the paleo-temperatures of the Central Andes and produced new estimates of lithospheric rigidity, which show that the elastic thickness of the Andean lithosphere varies spatially between ~5 and 50 km. Sedimentological and seismic stratigraphic studies by Uba et al. (2005, 2006) on the late Cenozoic strata in the Chaco basin delineated the sedimentary facies and architectures, depositional environments, and the spatiotemporal development of the basin. This data set includes isopach maps, which illustrate thickness distribution, geometry, and configuration of the Chaco basin since the late Cenozoic.

The sedimentary fill of foreland basins records both orogenic processes and lithospheric rheology, therefore the availability of new information on age of foreland basin strata, sedimentary thicknesses, sedimentation rates, geotherms, elastic thicknesses and structural history allows us to do a 2D flexural modelling along a W–E profile at approximately 21.4°S (Bolivian Central Andes) (Fig. 1). Many authors have previously applied 2D flexural models to study the evolution of the Andes as a whole (e.g., Flemings and Jordan, 1989; Toth et al., 1996; Horton and DeCelles, 1997; Cardozo and Jordan, 2001; DeCelles and Horton, 2003; Roddaz et al., 2005; Gómez et al., 2005) and the Chaco basin in particular (Lyon-Caen et al., 1985; Coudert et al., 1995; Watts et al., 1995; Ussami et al., 1999). Toth et al. (1996) postulated that the elastic thickness decreased dramatically with time (from 70 to 15 km) between 9 and 7 Ma along a profile at 22°S. They considered spatially constant elastic thickness along the studied profile. Likewise, the

* Corresponding author. Tel./fax: +5411 4788 3439.
E-mail address: prezzi@gl.fcen.uba.ar (C.B. Prezzi).

0040-1951/$ – see front matter © 2009 Elsevier B.V. All rights reserved.
doi:10.1016/j.tecto.2009.04.037

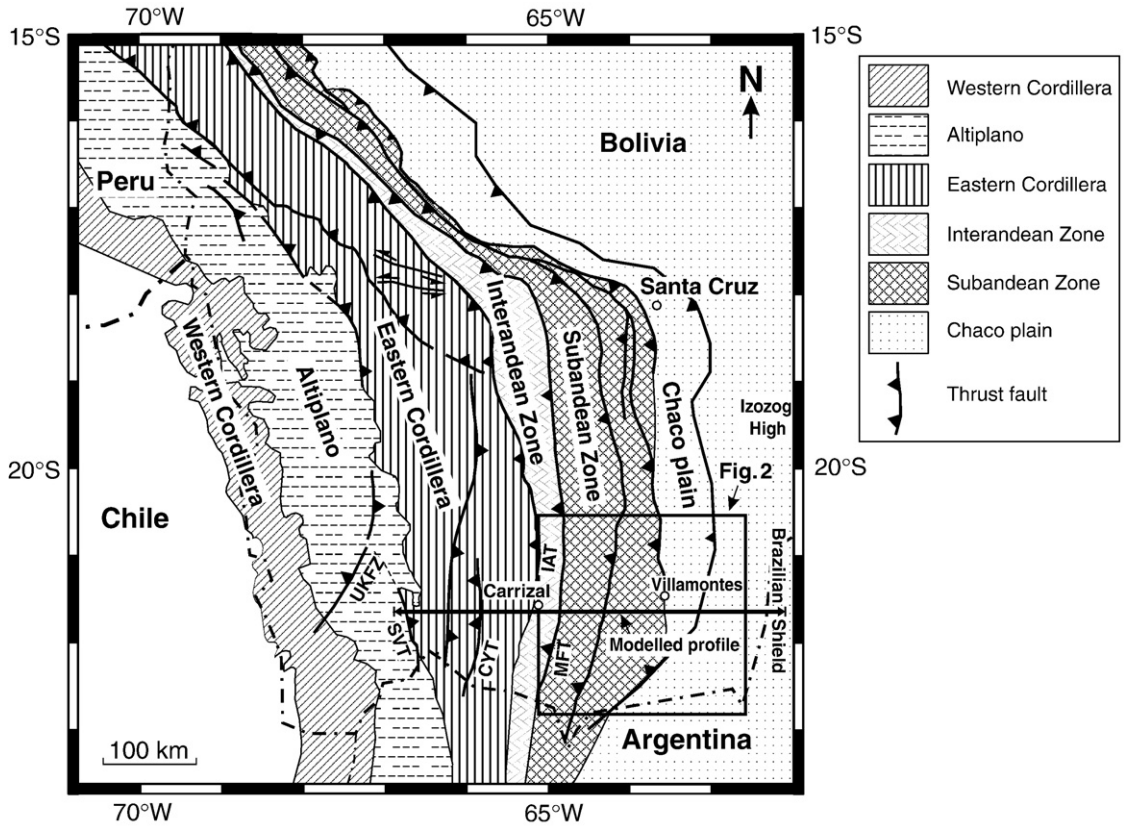

Fig. 1. Tectonic map of the Central Andes modified after Kley et al. (1997), Baby et al. (1995), 1997) and Müller et al. (2002) showing major morphotectonic divisions. The rectangular box indicates the study area as shown in Fig. 2. UKFZ: Uyuni–Khenayani Fault Zone, SVT: San Vicente Thrust, CYT: Camargo–Yavi Thrust, IAT: Interandean Thrust, MFT: Main Frontal Thrust. The solid black line shows the location of the modelled profile.

isostatic compensation applied by all the authors mentioned above assumes that the lithosphere behaves as a homogeneous elastic plate with laterally constant elastic thickness. In addition, the flexural estimates for the Chaco foreland basin were done with poorly constrained ages, thicknesses, and limited dataset. The newly published thickness maps, depocenter characterization, depositional ages of the late Cenozoic strata (Uba et al., 2005, 2006, 2007), estimates of elastic thickness (Tassara, 2005; Tassara et al., 2006) and detailed structural studies (e.g., McQuarrie, 2002; McQuarrie et al., 2005) provide a new opportunity to re-evaluate the flexural history of the Chaco Basin.

The objective of this paper is to investigate the relations between orogenic loading, erosion/sedimentation, flexural response, crustal strength, and associated foreland basin development. We use as input new estimates of elastic thickness (Tassara, 2005), sediment accumulation rates (Uba et al., 2007), timing, amount and style of structural shortening (e.g., McQuarrie and DeCelles, 2001; McQuarrie et al., 2005; Ege et al., 2007; Uba et al., 2009), and geotherms (Springer, 1999) to predict sedimentary thicknesses, basin geometries, crustal thicknesses, Bouguer anomaly, and topography for different evolutionary stages. The predictions are then compared to recently published sedimentary thickness and Chaco basin geometry (Uba et al., 2006, 2007). We assumed both elastic and elastic-plastic lithospheric rheologies and variation in rigidities in the modelled area. Through our model, we tried to evaluate if flexural processes can account for the documented subsidence, sedimentary thicknesses and depocenter migration in the study area. In addition, we attempted to test the occurrence of changes in elastic thickness during the basin development, as proposed by Toth et al. (1996). Our model permits a better understanding of the tectonic and dynamic interaction between the Chaco foreland basin and the Andean orogen, thus improving the comprehension of the driving mechanisms that resulted in the basin evolution.

2. Geological setting

2.1. Structural history

The Chaco foreland basin of south-eastern Bolivia consists of the Subandean Zone and the Chaco plain morphotectonic units (Figs. 1 and 2) (Uba et al., 2005). It is bounded on the west by the Main Frontal Thrust (MFT; Sempere et al., 1990) and on the east by the Brazilian Shield (Fig. 1). The basin development started since the late Oligocene with the migration of the forebulge depozone into the basin (Oller, 1986; Sempere et al., 1990; Uba et al., 2006). It represents the eastern expression of the Andean deformation at 50 Ma (DeCelles and Horton, 2003; Horton, 2005). The development of the Chaco basin is ultimately linked to the subduction of the Nazca plate under the South American plate coupled with simultaneous under-thrusting of the Brazilian Shield. This activity led to widespread and pronounced shortening in the Eastern Cordillera, which produced folding and eastward migration of thrusting (Baby et al., 1997; Allmendinger et al., 1997; Kley, 1996; Horton, 1998; McQuarrie, 2002; Ege et al., 2007). The consequence of this tectonism is eastward younging and migration of the depozones in time and space (DeCelles and Horton, 2003; Echavarria et al., 2003; McQuarrie et al., 2005; Horton, 2005; Uba et al., 2006).

Although it has been generally accepted that the deformation front arrived in the Chaco foreland basin at 10 Ma with the initiation of the Subandean Zone deformation (Gubbels et al., 1993; Moretti et al., 1996; Echavarria et al., 2003), Uba et al. (2007, 2009) show evidence for the arrival of the deformation front at 12.5 Ma. This proposition is in agreement with Horton (2005), who suggested an older age for the onset of the Subandean Zone deformation. In addition, at circa 12.5 Ma, the basin experienced high accommodation space creation, with relatively moderate sediment deposition

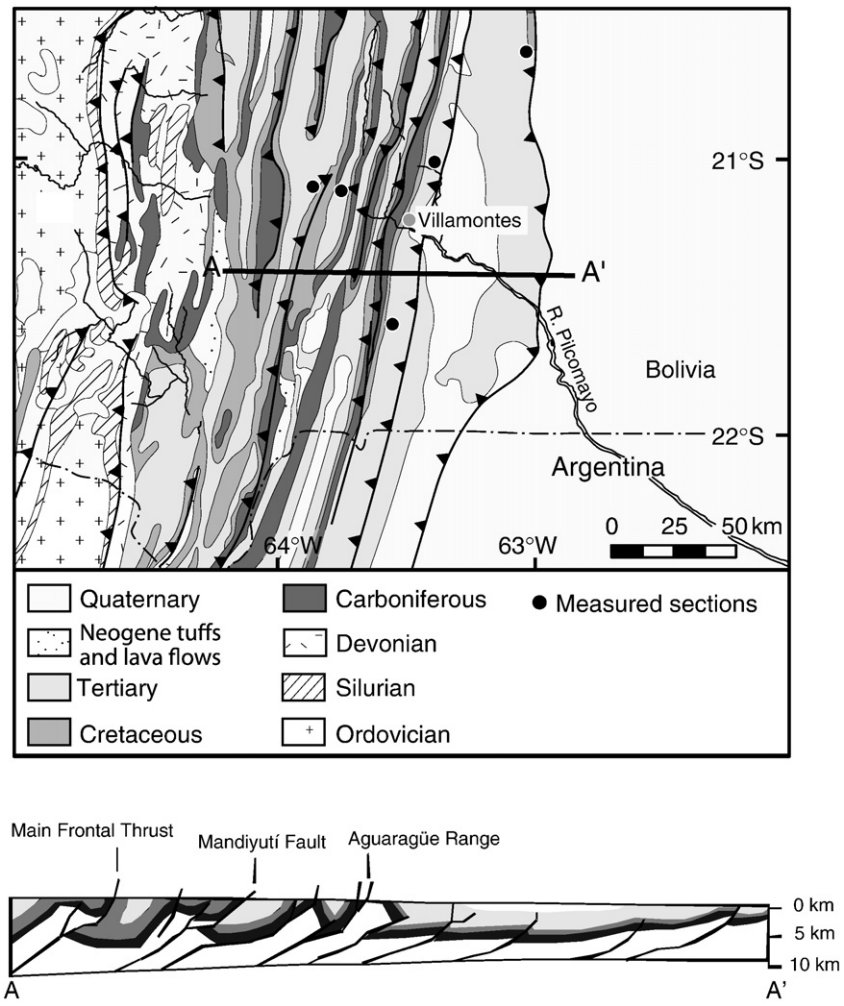

Fig. 2. General structural and geologic map of the Subandean Zone and Chaco plain modified from SERGEOMIN-YPFB 2002. Below is the structural cross-section diagram of AA′.

(Uba et al., 2005, 2006, 2007). Continuous deformation produced variable subsidence rates in the basin, with the highest subsidence rate recorded during the late Miocene (Coudert et al., 1995; Echavarria et al., 2003).

The Chaco foreland basin is characterized mostly by in-sequence, thin-skinned thrusting (Fig. 2) that includes ramp anticlines and passive roof duplexes (Baby et al., 1992; Dunn et al., 1995, Kley et al., 1999; McQuarrie, 2002) separated by thrust faults and synclines. However; Uba et al. (2009) documented out-of-sequence thrusting at circa 2.1 Ma in the basin. The main detachment levels for the thrusting are the Silurian- and the Devonian shales (Baby et al., 1992; Kley et al., 1999) (Fig. 2). The estimated total shortening in the Subandean Zone ranges between 67 and 100 km (Baby et al., 1997; McQuarrie, 2002; Ege, 2004; Barke and Lamb, 2006). The present deformation front is located in the central part of the Chaco plain.

2.2. Stratigraphy of the Chaco foreland basin

The geometry of the Chaco basin is asymmetric with a total stratigraphic thickness of more than 7.5 km of sedimentary rocks deposited in the deepest part at the west margin of the basin (Uba et al., 2005), while the foreland strata thins to the east (Uba et al., 2006). Recent regional sedimentological studies and new radiometric ages in the basin (Uba et al., 2005, 2006, 2007, 2009) have resulted in better understanding of the basin stratigraphy (Fig. 3). The late Cenozoic synorogenic strata are subdivided into five formations that unconformably overlie the Mesozoic eolian sandstones (Sempere et al., 1990; Dunn et al., 1995).

At the base of the foreland units is the late Oligocene to late Miocene 250-m-thick Petaca Formation. This formation consists mainly of basal paleosols, reworked pedogenic conglomerates, and sandstones that accumulated in a fluvial environment (Uba et al., 2005) (Fig. 3). According to Uba et al. (2006), the presence of a high-degree of pedogenesis indicates that during the deposition of the Petaca unit the basin was tectonically stable and experienced very low sediment accumulation. This formation represents deposition in a forebulge–backbulge depozone (Uba et al., 2005, 2006).

Overlying the Petaca Formation is the circa 500-m-thick Yecua Formation. These lacustrine-fluvial–shallow-marine strata compose mostly of mudstones and calcareous sandstones, which represent deposition in a distal foredeep depozone (Uba et al., 2005, 2006) (Fig. 3). A low-angle unconformity separates the Yecua Formation from the underlying Petaca Formation. Based on U–Pb dating on a tuff at the base of the Yecua Formation, the lower depositional age is constrained at 12.5 ± 0.24 Ma (Uba et al., 2007, 2009).

The up to 3000-m-thick fluvially deposited Tariquía Formation represents increased denudation and rapid increment in sediment accumulation in the medial foredeep (Uba et al., 2005, 2006) (Fig. 3). Sedimentological analysis indicates that rapid creation of accommodation space took place during the deposition of this unit (Uba et al., 2006, 2007). A U–Pb dating on zircon from volcanic ash at the base of the Tariquía Formation yielded 7.93 ± 0.09 Ma, thus placing the depositional ages at ~8 Ma (Uba et al., 2007, 2009).

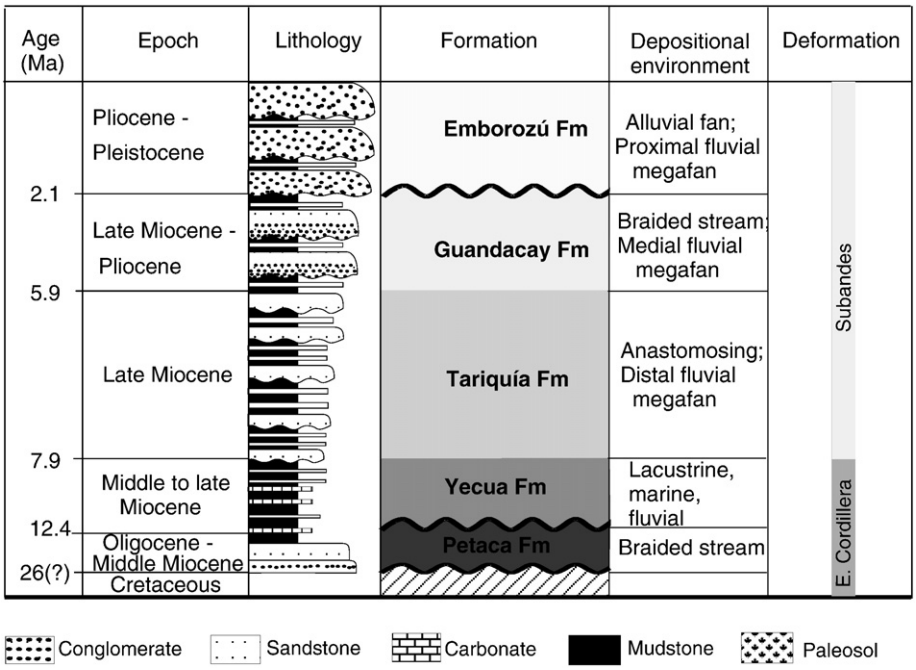

Fig. 3. Late Cenozoic lithostratigraphy of the Chaco foreland basin. The ages of the base of Petaca and Emborozú formations are based on Marshall and Sempere (1991) and Hulka (2005), respectively. The remaining ages are after Uba et al. (2007, 2009). The lithology shows an overall thickening and coarsening-upward sequence. The depositional environments are based on Uba et al. (2005, 2006). Deformation history after Uba et al. (2009).

The up to 1600-m-thick Guandacay Formation overlies transitionally the Tariquía Formation. The Guandacay Formation consists mainly of sandstones and conglomerates deposited in a medial fluvial megafan environment in a proximal foredeep depozone (Uba et al., 2005, 2006). Uba et al. (2007, 2009) placed the earliest depositional age at circa 6 Ma, which was based on 5.94 ± 0.08 Ma U–Pb-dated volcanic ash at its base (Fig. 3).

The late Cenozoic succession is capped by the more than 1500-m-thick Emborozú Formation, which is dominantly composed of conglomerates and sandstones deposited in a proximal fluvial megafan environment (Uba et al., 2005). This unit represents deposition in the wedge-top depozone due to eastward encroachment of the orogenic front (Uba et al., 2005, 2006). A dated volcanic ash near the base of this formation helped to constrain the earliest depositional age at 2.1 ± 0.54 Ma (Hulka, 2005), however, the upper depositional age is not constrained (Fig. 3).

3. The model

3.1. Theoretical framework and computing algorithm

Vening-Meinesz (1941) proposed a regional isostatic compensation model, which envisages an elastic plate that floats on a denser fluid substratum. A surface load (e.g., topography) bends the plate downward into the fluid substratum. The bending of the plate depends on the elastic properties of the lithosphere, e.g., rigidity. The resistance to bending of a thin elastic plate overlying a weak fluid is expressed by the flexural rigidity (D). A large value of D corresponds to a stiff plate. Considering the bending of a 2D thin elastic plate of thickness h, varying rigidity $D(x)$ and density δ_i, carrying a surface load $L(x)$, subjected to an externally applied horizontal stress P and supported by a substratum of density δ_m, the deflection of the plate at a position (x) relative to the centre of the load will be w (x):

$$\frac{d^2}{dx^2}\left[D(x)\frac{d^2w(x)}{dx^2}\right] + P\frac{d^2w(x)}{dx^2} + g(\rho_m - \rho_i)w(x) = L(x) \quad (1)$$

We used tAo software (Garcia-Castellanos et al., 1997) in the calculation of the flexural deflection of the lithosphere. This software is specially designed to model foreland basin formation, applying the finite-difference technique. The main advantages of this software, according to Garcia-Castellanos et al. (1997), are: (1) it uses time-varying load distribution (simulating thrust tectonics and orogen evolution) (Fig. 4); (2) it takes into account erosion and sedimentation processes, predicting large-scale geometry of the sedimentary infill; (3) it considers different lithospheric rheologies accounting for lateral variations of lithospheric rigidity or elastic thickness; (4) it allows the use of the elastic-plastic model and the concept of yield-stress envelope to calculate the elastic thickness (based on the method developed by Burov and Diament (1992, 1995)), therefore, permitting the comparison between elastic thicknesses calculated by completely different techniques and monitoring possible variations; and (5) it takes into consideration externally applied horizontal stresses to the plate.

This approach takes into account the structural evolution of the area, quantitatively reconciling sequential development of thrust sheet emplacement, foreland basin formation, and regional isostasy. Importantly, the foreland stratigraphy and basin accommodation space are directly coupled to thrust sheet development and lithosphere rheology. In the model, the geometry of each thrust fault is defined and the hanging wall is moved (Fig. 4a). This simple geometrical construction can be repeated to simulate shortening on multiple thrusts (Fig. 4c). Different thrust load densities and geometries (e.g., dip angle, detachment depth) result in distinct isostatic subsidence and basin accommodation space for the same amount of shortening.

The choice of this numerical modelling approach over simple flexural models is based on its ability to simulate structural evolution instead of using static instantaneous loads, and on the possibilities of considering erosion–sedimentation processes, different rheologies and varying rigidities. These characteristics permit the reproduction of a more realistic model of the basin evolution and the investigation of the relationships between basin stratigraphic development, thrust loading and rheology.

Time-dependent processes are calculated in two repeated steps: load redistribution and plate deflection. To further constrain the final

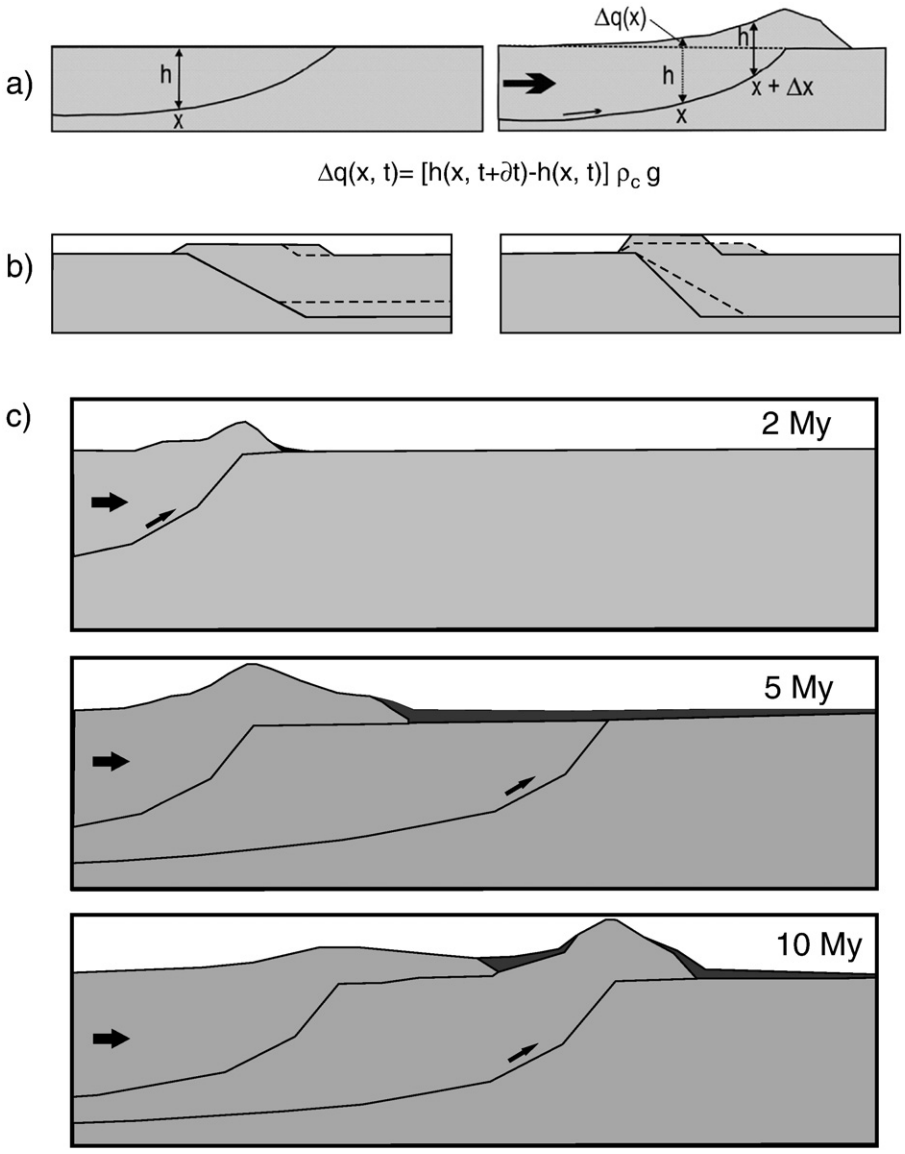

Fig. 4. a) Thrust sheet emplacement and the corresponding loading. The model is kinematically driven, we introduce the position, geometry, period of activity and rate of shortening. A listric geometry with a horizontal detachment depth is assumed. Once the fault is defined, the hanging wall is moved horizontally (acting as a simple moving load) and collapsed onto the footwall (Toth et al., 1996). b). Left: Cartoon showing the effect on the topography of fault detachment depth variation. Dotted (solid) line: shallow (deep) detachment level. Right: Cartoon showing the effect on the topography of fault dip angle variation. Dotted (solid) line: small (large) dip angles (modified from Gaspar-Escribano and Garcia Castellanos, 2004). c) Example showing the evolution along time of a simple model corresponding to shortening on multiple thrusts. Dark grey: Sedimentary deposits.

crustal geometry, tAo computes gravity anomalies corresponding to the final mass distribution using the algorithm of Talwani et al. (1959) (Garcia-Castellanos et al., 1997). The gravity field is assumed to be affected only by crustal geometry, load units (thrusts), sediment and water. The following processes and aspects are taken into account in the numerical modelling performed with tAo (Garcia-Castellanos et al., 1997): thrust sheet loading, erosion, sedimentation, and rheology.

3.1.1. Thrust sheet load

The model is kinematically driven, with the position, geometry, and movement of each fault prescribed. Given the geometry of a fault, the hanging wall is moved according to the corresponding shortening rate and period of activity (Fig. 4a). The hanging wall is collapsed by vertical shear onto the footwall (Fig. 4a), while the vertical thickness of the hanging wall block is preserved during fault movement (Fig. 4a). The shape of the topography resulting from tectonic transport along a fault plane depends on the fault geometry (Gaspar-Escribano and Garcia Castellanos, 2004). For the same amount of shortening and dip angle, the deeper the detachment level, the wider the topography created by thrusting (Fig. 4b). Similarly, for the same amount of shortening and depth of the detachment level, the higher the dip, the higher and narrower the resulting topography (Fig. 4b). This simple geometrical construction is sequentially repeated to simulate shortening on multiple thrusts (Fig. 4c).

3.1.2. Erosion–sedimentation

The topography produced by thrusting and modified by regional isostatic response of the lithosphere is used at each time step to calculate erosion and sedimentation considering three simple models (Garcia-Castellanos et al., 1997):

(a) Continental subaerial denudation rate (CE) is assumed to be proportional to topographic height $h(x, t)$ and erosion rate (k_{ce}):

$$CE = -\, k_{ce} h(x,t) \text{ for } h(x,t) > 0; \quad (2)$$

(b) Sedimentation rate (SS) is constant in space and time under sea level with a linear decrease at shallowest depths:

$$SS = k_{ss}[h(x,t) / h_1] \text{ for } h_1 < h(x,t) < 0 \quad (3)$$

$$SS = k_{ss} \text{ for } h(x,t) \leq h_1 \text{ with } h_1 = -k_{ss}dt \quad (4)$$

where k_{ss} is the maximum sedimentation rate and h_1 is the depth above which sedimentation changes gradually from k_{ss} to 0 (h_1<0). This linear decrease of sedimentation is used to avoid the deposition of sedimentary thicknesses greater than the water depth (h) during a time interval (dt). To reproduce subaerial continental sedimentation, the level dividing erosion and sedimentation is raised above sea level (e.g. 100 m in Garcia-Castellanos et al., 2002).

(c) Diffusive erosion/sedimentation (DES) is also applied:

$$DES = \alpha\left[\partial^2 h(x,t) / \partial x^2\right] \quad (5)$$

where α is the diffusion transport coefficient, usually circa 10^6 m^2/Ma (Flemings and Jordan, 1989).

The total topography variation rate is: $\partial h(x,t) / \partial t = CE + SS + DES$.

The space available below sea level is determined by four factors: the initial plate height, the topographic relief created by thrusting, the rates of erosion and sedimentation, and the regional flexural subsidence (Garcia-Castellanos et al., 1997). To reproduce the infill of the basin with continental sediments, the level dividing erosion and sedimentation can be raised above sea level according to the average altitude of the modelled foreland basin (Garcia-Castellanos et al., 2002).

3.1.3. Rheology

In our model, we considered pure elastic and elastic-plastic depth-dependent rheologies, and compared the corresponding results.

The pure elastic rheology assumes that plate bending stresses are distributed linearly with depth, and will completely recover to the original state when the load is removed. The only parameter required to describe the mechanical behaviour of a two-dimensional elastic thin plate is its elastic thickness (Watts, 2001; Turcotte and Schubert, 2002). The elastic-plastic rheology considers a recoverable linear distribution of stress limited by the yield-stress envelope. To calculate the lateral variations of elastic thickness of the flexed lithosphere, the method described by Burov and Diament (1992, 1995) is used. The input data for this model are the thermal regime, crustal geometry and rheological parameters (standard values were taken from Lynch and Morgan (1987) and Zeyen et al. (1996)). These parameters define the yield-stress envelope or strength profile of the lithospheric plate that controls the stress distribution. The code also accounts for the mechanical coupling or decoupling between crust and mantle (Garcia-Castellanos et al., 1997).

3.2. Model setup

The modelled W–E profile runs along 21.4°S, extending from 66.9°W for 1250 km to the east (Fig. 1). We applied a semi-infinite plate model with a plate fracture located at 66.9°W, 70 km east of the San Vicente Thrust (SVT), beneath the eastern Altiplano–western Eastern Cordillera (Fig. 1). Watts et al. (1995) used a similar position for the plate fracture in their modelling. Such a position is justified considering that ductile flow in the lower crust beneath the western margin of the Eastern Cordillera has been proposed by different authors to explain uplift and estimated shortening (e.g., Beck and Zandt, 2002).The following data and parameters were used as input to compute the 2D flexural model: structure, erosion and sedimentation rates, densities and rheology (Table 1).

Table 1
Model input parameters and data.

Length of the model	1250 km		
Modelled time span	40–0 Ma		
Time step	0.25 My		
Gridding			
Number of x points (distance axis)	1250		
Number of z points (depth axis for elastic-plastic model)	751		
Mechanical parameters			
E (Young's modulus)	7×10^{10} N/m^2		
ν (Poisson's ratio)	0.25		
Densities			
Sediments	2200 kg/m^3		
Crust	2900 kg/m^3		
Mantle	3330 kg/m^3		
Loads	2800 kg/m^3		
Water	1020 kg/m^3		
g (acceleration of gravity)	9.81 m/s^2		
Input data			
	Shortening	Number of thrusts	Time of thrust activity
Structure			
Eastern Cordillera	50 km	8	40–30 Ma
Interandean Zone	40 km	9	30–11 Ma
Subandean Zone	100 km	12	11–0 Ma
First basement megathrust	280 km		30–29 Ma
Second basement megathrust	330 km		10–9.5 Ma
Erosion and sedimentation			
α (diffusion transport coefficient)	3×10^9 m^2/My		
k_{ce} (erosion rate)	0.01 m/mMy		
k_{ss} (maximum sedimentation rate)			
Petaca Formation	2 m/My		
Yecua, Tariquía, Guandacay and Emborozú Formations	200 m/My		
Rheology			
Initial crustal thickness	35 km		
Initial upper crustal thickness	15 km		
Geotherms	Springer (1999): Eastern Cordillera, Subandean belts and Chaco plain geotherms before deformation		
Elastic thickness	Tassara (2005): Profile 5: ~22.6°S		

3.2.1. Structure

In the modelling, we assume listric geometries with horizontal detachment depths. Once the fault is defined, the hanging wall is moved horizontally (acting as a simple moving load) and collapsed onto the footwall (Toth et al., 1996). The vertical thickness of the hanging wall block is preserved during fault movement (Fig. 4a). The width and height of the topography resulting from tectonic transport along the fault plane for a given amount of shortening, depend on the geometry of the fault (Gaspar-Escribano and Garcia Castellanos, 2004) (Fig. 4b). This procedure is sequentially repeated to reproduce shortening on multiple thrusts and propagation of the deformation front towards the foreland (Fig. 4c).

In order to define the thrust loading process through time along the modelled profile, we considered that the Eastern Cordillera underwent shortening of 50 km between 40 and 30 Ma, the Interandean Zone was shortened 40 km between 30 and 11 Ma and the Subandean Zone experienced shortening of 100 km between 11 and 0 Ma (e.g., Kley et al., 1997; Ege, 2004) (Table 1). We used the restored balanced cross-sections of Kley et al. (1997) and McQuarrie and DeCelles (2001); which show the pre-thrust situation; to define the number, geometry and location of the thrusts included in our model. The above-mentioned shortening was distributed among in-sequence east-verging thrusts: 8 in the Eastern Cordillera, 9 in the Interandean Zone and 12 in the Subandean Zone (Table 1). Additionally, the

propagation of two major basement megathrusts sheets (McQuarrie and DeCelles, 2001) was included in the model. The geometry and location of the unmoved faults (pre-thrusting) used as input in our model are shown in Figs. 6a and 9 (top). The timing of deformation and the amount of shortening corresponding to each fault are presented in Table 2.

3.2.2. Erosion, sedimentation, and densities

Barnes and Pelletier (2006) reported long-term denudation rates across the eastern Bolivian Andes (14–22°S) from thermochronology, cosmogenic radionuclides, foreland basin sediment volumes, stratigraphy, and paleoerosion surface degradation. They showed that denudation rates averaged over the last ~10 Ma range from 0.04 to 0.33 mm/yr for the zone studied here. Furthermore, these authors noted that average denudation rates that integrate over more than the last ~10 Ma should be lower than those estimates that do not, and that denudation rates may be increasing to the present. Taking into account the time span (40 to 0 Ma) modelled in this work, we considered 0.04 mm/yr as a maximum limit for the denudation rate, therefore, we used this value to estimate the erosion rate of 0.01 m/mMy (Table 1) (Eq. (2)).

We calculated the transport diffusion coefficient from Eq. (5), considering the average topographic slope and the volume of foreland basin fill (Uba et al., 2005, 2006) along the modelled profile. The obtained value is very similar to the one estimated by Flemings and Jordan (1989), in light of this, we used a transport diffusion coefficient of 3×10^9 m^2/My (Table 1).

Average sedimentation rates for: Petaca Formation: 2 m/My, Yecua, Tariquía, Guandacay and Emborozú Formations: 200 m/My by Uba et al. (2005, 2006) were used (Table 1).

The available space for sediment deposition is determined by the initial plate height, the topographic relief created by thrusting, the rates of erosion and sedimentation, the regional flexural subsidence, and the sea level (Garcia-Castellanos et al., 1997). In addition, we used the global sea level curve of Haq et al. (1987) recalibrated to Berggren et al. (1995) timescale. As mentioned in Section 2.2, most of the Formations modelled here were deposited in fluvial environments (except for the lacustrine–shallow-marine strata of Yecua Formation). Terrestrial (megafan-fluvial) depositional conditions are modelled considering that the level separating erosion and sedimentation progressively diminished from 100 m to 0 m above sea level during the deposition of Petaca Formation; that it was at 0 m elevation during the time of deposition of Yecua Formation; and that it progressively raised from 0 m to 200 m above sea level between 8 and 0 Ma, based on the ages of the Tariquía, Guandacay and Emborozú Formations. The sedimentation level of 200 m above sea level corresponds to the average present altitude of the Chaco foreland basin.

In addition, we applied the following densities; sediments: 2200 kg/m^3, crust: 2900 kg/m^3, mantle: 3330 kg/m^3, loads: 2800 kg/m^3.

3.2.3. Rheology

We applied two different rheological behaviours for the lithospheric plate; pure elastic and depth and temperature dependent elastic-plastic.

In the first case, varying values of elastic thickness along the profile were considered. We used the present-day values proposed by Tassara (2005, profile 5: ~22.6°S) (Fig. 5a), which increase from 13 km in the western to 60 km in the eastern extremes of our profile. Tassara (2005) carried out a two-dimensional flexural analysis based on the correlation between topography and Bouguer anomaly. In such analysis an iterative change both in the elastic thickness and the value of total horizontal stress allowed the best visual fit between measured and model-generated Bouguer anomalies. Only the effects of vertical topographic loads were considered.

On the other hand, the input data for the elastic-plastic model are the thermal regime, crustal geometry and rheological parameters. The initial geotherms for the Eastern Cordillera, the Subandean Zone, and the Chaco plain estimated by Springer (1999) before deformation were used (Fig. 5b). For the Eastern Cordillera and the Subandean Zone, Springer (1999) applied a 2D crustal stacking model considering surface heat flow densities of 60 mW/m^2 and 45 mW/m^2, respectively. In contrast, the same author used a 1D geotherm model for the Chaco plain considering that surface heat flow density ranges between 40 and 56 mW/m^2. Initial crustal thickness of 35 km (e.g., Husson and Sempere, 2003) and initial upper crustal thickness of 15 km (e.g., Yang et al., 2003) were used. According to the depth and temperature dependent elastic-plastic rheology, the lithosphere behaves elastically below a certain yield stress that varies in depth. When this yield stress is reached, anelastic deformation takes place. The maximum stress that crustal and mantle rocks can resist without undergoing permanent deformation is governed by the following equations (Lynch and Morgan, 1987)

$$\text{Brittle deformation:}\quad \sigma_{y-b}(z) = Bz \tag{6}$$

$$\text{Ductile deformation:}\quad \sigma_{y-d}(z) = \left(\frac{\dot{\varepsilon}}{A}\right)^{\frac{1}{n}} \exp\left(\frac{Q}{nRT}\right) \text{ when } \sigma \leq 200 \text{ MPa} \tag{7}$$

$$\sigma_{y-d}(z) = \sigma_d\left[1-\left(\frac{RT}{Q_d}\ln\left(\frac{\dot{\varepsilon}_d}{\dot{\varepsilon}}\right)\right)^{1/2}\right] \text{ when } \sigma > 200 \text{ MPa} \tag{8}$$

Table 2
Input fault configuration.

Fault	Start (Ma)	End (Ma)	Shortening (km)
Eastern Cordillera			
1	40	39	6.25
2	38.75	37.75	6.25
3	37.5	36.5	6.25
4	36.25	35.25	6.25
5	35	34	6.25
6	33.75	32.75	6.25
7	32.5	31.5	6.25
8	31.25	30.25	6.25
First basement megathrust			
9	30	29	280
Interandean Zone			
10	28	27	4.44
11	26	25	4.44
12	24	23	4.44
13	22	21	4.44
14	20	19	4.44
15	18	17	4.44
16	16	15	4.44
17	14	13	4.44
18	12	11	4.44
Second basement megathrust			
19	10	9.5	330
Subandean Zone			
20	9.25	8.75	20
21	8.5	8	15
22	7.75	7.25	19
23	7	6.5	3.5
24	6.25	5.75	3.5
25	5.5	5	5
26	4.75	4.25	10
27	4	3.5	10
28	3.25	2.75	5
29	2.5	2	3
30	1.75	1.25	3
31	1	0.5	3

Start and End refer to fault activity periods. Shortening is measured in the horizontal direction.

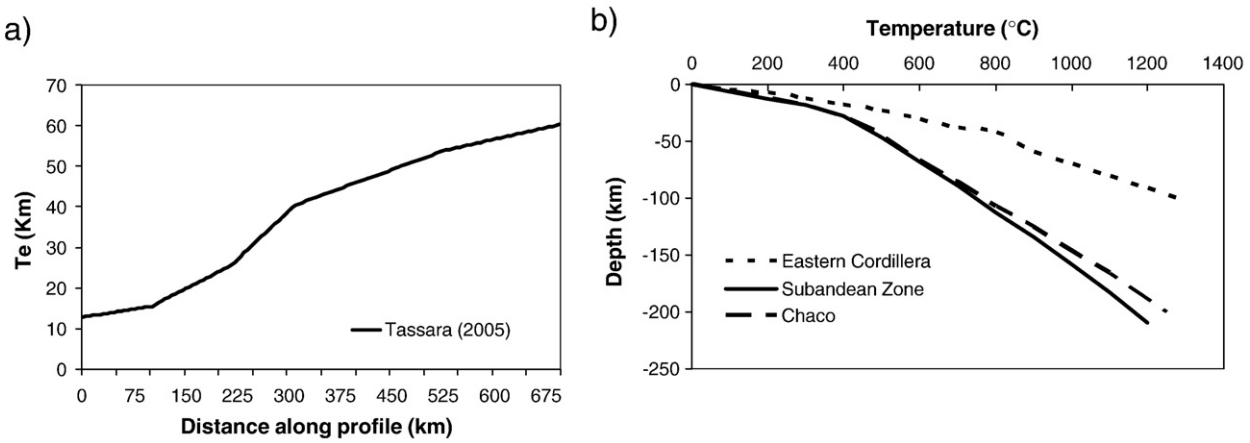

Fig. 5. a) Elastic thickness along ~22.6°S, calculated by Tassara (2005, profile 5), b) initial geotherms for Eastern Cordillera, Subandean Zone and Chaco plain estimated by Springer (1999) before deformation.

where $\sigma_{y\text{-}b}$ and $\sigma_{y\text{-}d}$ are brittle and ductile yield stress respectively, σ is applied stress, z is depth, B is the brittle yield-stress gradient (16 MPa/km for extension and 40 MPa/km for compression, Lynch and Morgan, 1987), R is the gas constant, T is the absolute temperature, $\dot{\varepsilon}$ is the effective strain rate (we assumed a value of 10^{-16} s^{-1}) and A, Q, n, σ_d, Q_d and $\dot{\varepsilon}_d$ are material constants depending on the rock-type. We have considered that the upper crust has a quartz-rich composition, that the lower crust has an intermediate composition between diabase and diorite and that the lithospheric mantle is represented by an olivine-dominated lithology. In this work we have used representative rheological parameters (Table 3) taken from Lynch and Morgan (1987) and assumed that crust and mantle are mechanically decoupled.

3.3. Limitations and simplifications of the modelling

There are certain limitations and simplifications in our modelling, for example, out-of-sequence thrusts and thrusts with opposite vergence could not be modelled. In addition, it is not possible to consider thrust reactivations during the structural evolution. Erosion and sedimentation rates are considered constant in space and time; therefore, they could not be varied along the profile or during the temporal evolution (i.e. during a model run). Variations of erosion rates would affect topographic elevation and, consequently, would produce changes in the basin amplitude (i.e. basin depth). Changes in sedimentation rates would generate variations in the thickness of the sedimentary units deposited in the basin; however, such thickness is limited to a maximum value according to the available accommodation space.

Conversely, the accommodation space is mainly controlled by the geometry and density of the orogenic and sedimentary loads, the lithospheric strength, and the horizontal stress. Importantly, the wavelength of the basin (i.e. basin width) depends on the lithospheric rigidity and the horizontal stress (Watts, 2001). Therefore, variations in the erosion and sedimentation rates can induce changes in the basin depth (i.e. amplitude), but they cannot induce changes in the basin width (i.e. basin wavelength) (Watts, 2001). Elastic thicknesses, geotherms, and initial crustal thicknesses can change in space; nonetheless, they remain constant during temporal evolution. Interestingly, the model can be stopped at any time, permitting the possibility to use different parameters to model the evolution at different time intervals. Regarding these limitations and simplifications, it should be taken into account that in our approach we did not intend to predict detailed geometries, but to reproduce large-scale features.

3.4. Comparing model predictions to "reality"

The structural geometry and shortening considered in our model should produce sufficient thrust sheet loading and foreland subsidence to accommodate the observed foreland stratigraphy. The model should also accurately predict the large-scale architecture of the foreland basin stratigraphic units, the observed topography, crustal thickness and Bouguer anomaly. In this study we attempt to: (1) use a simple modelling approach to determine the possibility of reproducing the present-day foreland Chaco basin system based on the available structural, sedimentary, and rheological information; (2) test the depozone characterizations of the Chaco basin stratigraphic units documented by Uba et al. (2006); (3) test the occurrence of changes in elastic thickness during the basin development, as those proposed by Toth et al. (1996), and (4) obtain new insight into the development of the Chaco basin and the evolution of the Andean orogen.

The predicted topography is compared with actual topography derived from digital elevation models (GTOPO30). New stratigraphic data obtained from industry seismic reflection profiles, well logs, and field section measurements in the Chaco basin (Uba et al., 2005, 2006) are used for comparison with our modelled sedimentary thicknesses. The calculated gravity anomalies corresponding to the final mass distribution modelled along the profile are compared with the corresponding measured values (Götze et al., 1990; Götze and Kirchner, 1997; Prezzi et al., in press). Elastic thicknesses calculated along the modelled profile assuming elastic-plastic rheology are compared with those based on flexural analysis of the correlation between relief and gravity by Tassara (2005, profile 4: ~19.6°S and profile 5: ~22.6°S). Predicted Moho depths are compared with values of crustal thickness calculated from seismic (Yuan et al., 2002) and gravimetric data (Tassara, 2005, profile 5: ~22.6°S).

4. Results

Our modelling goes forward with time, beginning at 40 Ma, when the initial kinematic conditions are constrained by the restored pre-

Table 3
Rheological parameters used for crust and mantle in the elastic-plastic model (Lynch and Morgan, 1987).

	A (MPa^{-n} s^{-1})	Q (kJ/mol)	n	Q_d (kJ/mol)	σ_d (MPa)	ε_d (s^{-1})
Upper crust	2.5×10^{-8}	140	3			
Lower crust	3.2×10^{-3}	250	3			
Lithospheric mantle	7×10^{4}	520	3	545	8.5×10^{3}	5.7×10^{-11}

thrusting structural geometry (Fig. 6a), and terminating at 0 Ma as the thrusting migrated into Chaco (Fig. 6f). The modelled section is sequentially shortened. Fig. 6 shows the different evolutionary stages of the fold and thrust belt and the corresponding foreland basin system at 40, 30, 20, 14, 6 and 0 Ma. Tables 1–3 show the model parameters and input data (e.g., amount of shortening, number of thrusts, time of activity of each modelled thrust, and sedimentation rates). Taking into account the recently published new ages and isopach maps by Uba et al. (2006, 2007), we modelled foreland basin evolution at 14 Ma (only Petaca Formation was deposited), 6 Ma (Petaca, Yecua and Tariquía Formations were deposited), and 0 Ma (Petaca, Yecua, Tariquía, Guandacay and Emborozú Formations were deposited). Thus, we compared the model predictions with the corresponding data (see Section 3.4). The results predicted by our

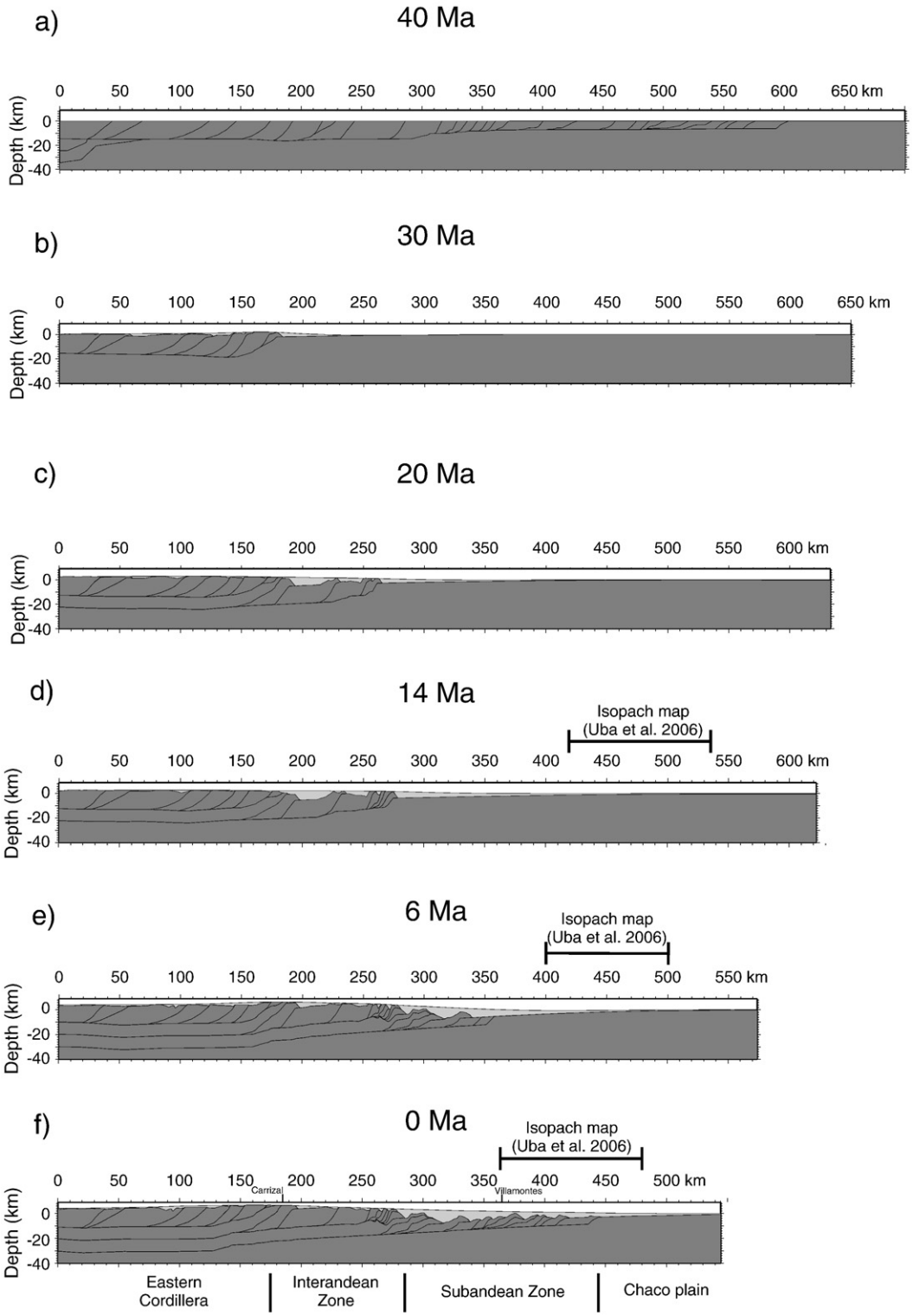

Fig. 6. Modelled structural setting, basin geometry, topography and sedimentary thicknesses for: a) 40 Ma, b) 30 Ma, c) 20 Ma, d) 14 Ma, e) 6 Ma and f) 0 Ma evolutionary stages. On the first undeformed section (40 Ma) the unmoved faults are shown for comparison with the subsequent times. The location of the isopach maps produced by Uba et al. (2006) for each stage is shown. The approximate location of Carrizal and Villamontes is shown. Pale gray: Cenozoic sedimentary units.

0 Ma evolutionary stage model compare to a variety of data, in contrast to 6 Ma and 14 Ma evolutionary stages, whose predictions can only be compared to measured sedimentary thicknesses. We will present the results for 0, 6, and 14 Ma stages, respectively.

4.1. 0 Ma evolutionary stage

At this stage, Petaca, Yecua, Tariquía, Guandacay and Emborozú Formations were already deposited (Fig. 6f). Fig. 7 shows the comparison between our model predictions and the corresponding "real" data (topography, Bouguer anomaly, Moho depths, sedimentary thicknesses and elastic thicknesses) for the final stage (0 Ma), assuming elastic-plastic rheology. We modelled the same system again, however, using elastic rheology as shown in Fig. 8.

The results obtained from both rheologies are similar, as shown in Figs. 7 and 8. The measured and modelled Bouguer anomalies fit well. Modelled Moho depths, which decrease from 51 km beneath the Interandean Zone to 35 km beneath the Chaco plain, show a very good fit with the estimations of Tassara (2005). In contrast, the depths obtained by Yuan et al. (2002) are approximately 5–10 km deeper (Figs. 7 and 8). Allmendinger et al. (1997) and Giese et al. (1999) pointed out that the deeper Moho imaged by seismic methods can be related to the transition between a serpentinized and an anhydrous subcrustal mantle and not to the petrologic crust–mantle boundary. Serpentinization generates greater reduction of seismic velocities than of densities. Modelled altitudes are higher than GTOPO30 elevations for the Eastern Cordillera and Subandean Zone, however, lower for the Chaco plain (Figs. 7 and 8). In addition, we observed that the predicted topography along the profile is too smooth. Nevertheless, considering the limitations and simplifications of the model, the obtained fit is fairly good.

The model predicts maximum sedimentary thicknesses of ~6000 m, which is in agreement with measured values (Uba et al., 2005, 2006) (Figs. 7 and 8). Interestingly, there is a very good fit between the modelled variation of sedimentary thickness along the profile and the thicknesses documented by Uba et al. (2006) for the Chaco foreland basin. The "saw-toothed" variation in modelled thicknesses registered in the western part of the profile (Figs. 7 and 8) indicates the existence of unconformities and erosion generated by the propagation of the deformation front in the present Subandean Zone, and thus, reflecting the existence of "sub-basins" between the modelled thrusts. Uba et al. (2006) recognized the possible existence of "sub-basins" in the Emborozú Formation based on sedimentological and basin analysis. Importantly, the final sedimentary thicknesses are iteratively calculated for each unit from erosion and sedimentation. The sediment fill between the thrusts creates the smooth topography and the irregular

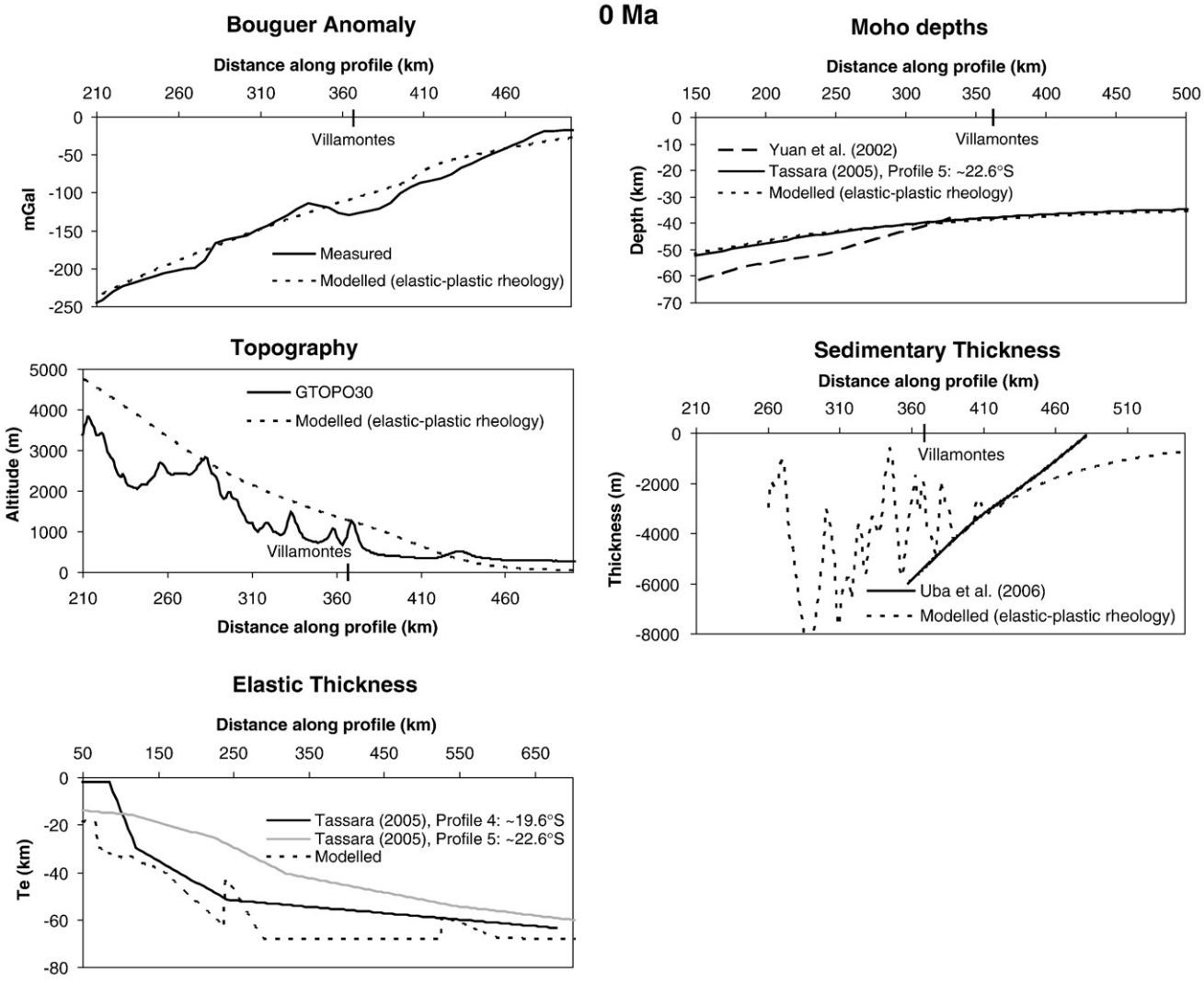

Fig. 7. Comparison between our model predictions and the "real" data for the final stage of the Andean evolution (0 Ma), assuming elastic-plastic rheology. From top to bottom and from left to right: Bouguer anomaly, Moho depths, topography, sedimentary thickness, and elastic thickness. The approximate location of Villamontes is shown.

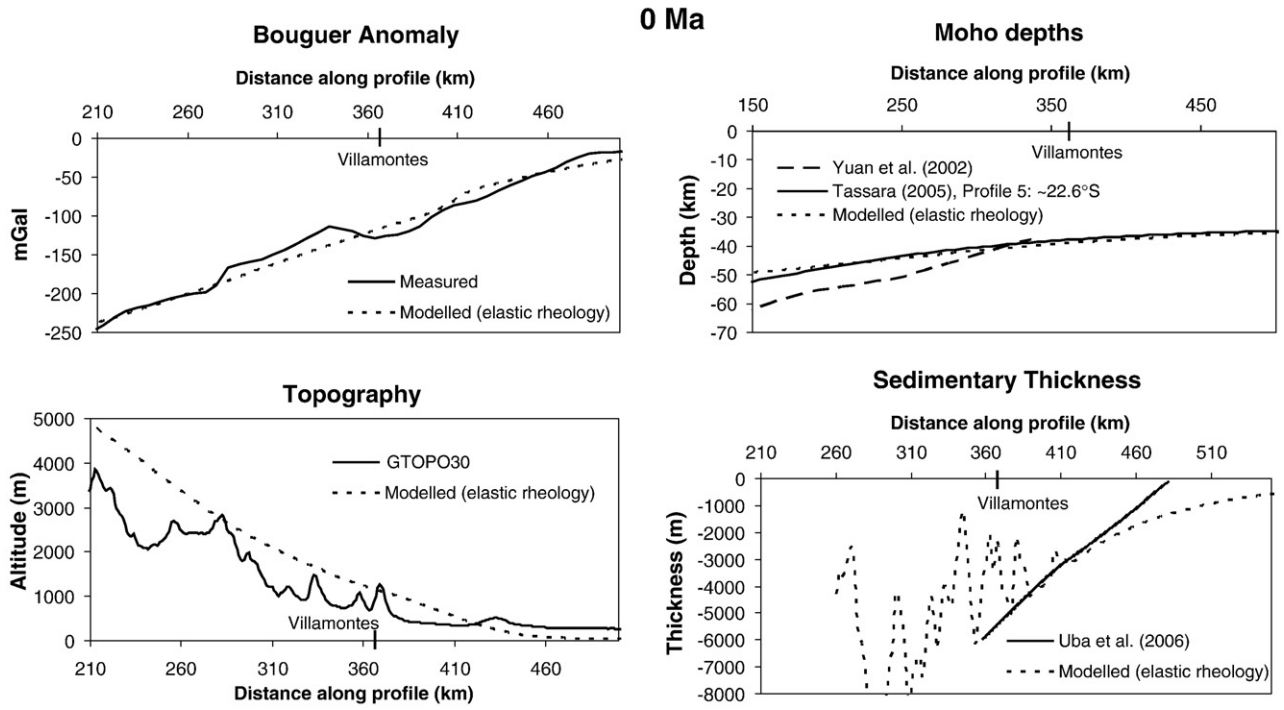

Fig. 8. Comparison between our model predictions and the corresponding "real" data for the final stage of the Andean evolution (0 Ma), assuming elastic rheology and using as input the elastic thicknesses estimated by Tassara (2005). From top to bottom and from left to right: Bouguer anomaly, Moho depths, topography and sedimentary thickness. The approximate location of Villamontes is shown.

sedimentation pattern in our model. The deformation front is at ~410 km and the modelled basin width is of ~270 km (Fig. 6f). The existence of wedge-top (between 260 and 410 km) and proximal foredeep (~from 410 km to the east) depozones can be interpreted (Figs. 6f–8). This interpretation is in agreement with the wedge-top and proximal foredeep depozones proposed by Uba et al. (2006) for Emborozú and Guandacay formations respectively.

The modelled elastic thicknesses, assuming elastic-plastic rheology and using geotherms as input, showed an increase from 18 km in the Eastern Cordillera to 68 km in the Chaco plain (Fig. 5b). These values are higher than the estimations of Tassara (2005) (Fig. 7). The discrepancy between the two estimates could be related to biases of the thermal model (Springer, 1999) or the initial crustal structure that is used as input for the calculation. Nevertheless, the obtained elastic thicknesses show a good fit with the values reported by Tassara (2005) along ~19.6°S (Fig. 7). Moreover, the general trend of our modelled elastic thickness, which increases from west to east, is in agreement with previous estimates (e.g., Watts et al., 1995; Stewart and Watts, 1997; Tassara et al., 2006). Watts et al. (1995) showed that along ~21°S the elastic thickness varies from less than 25 km beneath the Altiplano, to ~50–60 km in the Subandean Zone, and up to 75 km in the Chaco plain. Furthermore, Coudert et al. (1995) estimated elastic thicknesses beneath the western Chaco plain at ~20°S between 29 and 31 km. Stewart and Watts (1997) suggested that the elastic thickness along ~22°S changes from 25 km in the Altiplano to 50 km in the Subandean Zone and the Chaco plain. The breaks observed in the modelled elastic thickness (at ~250 and 550 km) (Fig. 7) correspond to interpolation artifacts, which coincide with the positions along the profile of the geotherms used as input.

As mentioned in Section 3.2.1, we used the restored- (pre-thrusting) cross-sections of Kley et al. (1997) and McQuarrie and DeCelles (2001) to constrain the number, geometry, and location of the thrusts in our model. In order to test the ability of the model to replicate the actual structural setting along the profile, we compared the structural configuration obtained at the end of the model with the geological (post-thrusting) cross-section of McQuarrie and DeCelles (2001) (Fig. 9). Although the obtained structural configuration differs markedly in detail from the geological (post-thrusting) cross-section of McQuarrie and DeCelles (2001), large-scale features (e.g., basement megathrust thickness, depth of major detachment levels) are reasonably reproduced by our model. Considering the limitations and simplifications of the modelling (see Section 3.3) and the simple geometrical construction used to simulate shortening (see Section 3.1.1), which determines the final location of the faults in our model, the obtained match is regarded as acceptable. Bearing in mind that with our approach we do not intend to predict detailed geometries, but to reproduce large-scale features, the attained fit validates our results.

4.2. 6 Ma evolutionary stage

At this stage (Fig. 6e) Petaca, Yecua and Tariquía Formations were already deposited. Fig. 10 shows modelled vs. measured sedimentary thicknesses along the profile at 6 Ma. At 6 Ma, the model showed that maximum sedimentary thicknesses of circa 7000 m were obtained for the wedge-top/foredeep depozone (~330 km, Figs. 6e and 10) to the west of the area studied by Uba et al. (2005, 2006). The "saw-toothed" variation in modelled thicknesses registered in the western part of the profile (west of 335 km) (Figs. 6e and 10) indicates the existence of unconformities and erosion generated by the propagation of the deformation front. The deformation front is at ~350 km and the modelled basin width is ~230 km (Fig. 6e). There is a good correspondence between the modelled variation of sedimentary thickness along the profile and the sedimentary thicknesses estimated by Uba et al. (2006), which range between ~2300 and 500 m (Fig. 10). We interpret the non existence of unconformities or erosional surfaces and the modelled basinwide geometry along the profile studied by Uba et al. (2006), as indicative of deposition in a medial–distal foredeep depozone (see Fig. 6e). This interpretation is consistent with the high subsidence rates and increment in accommodation space documented in the study area (Coudert et al., 1995; Echavarria et al.,

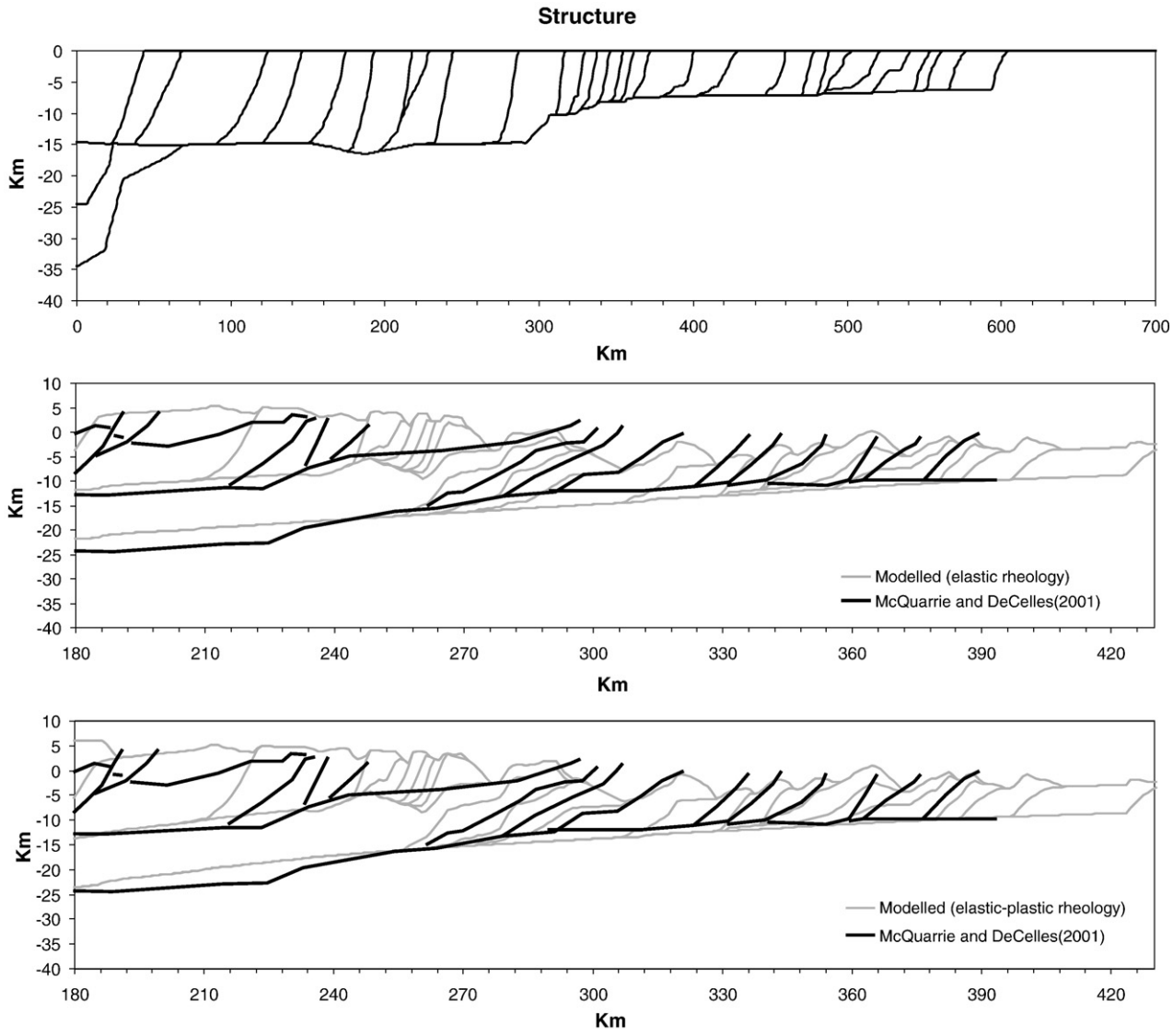

Fig. 9. Top: Unmoved structural setting (pre-thrusting) used as input in our model (based on the cross-sections of Kley et al. (1997) and McQuarrie and DeCelles (2001)). Middle and bottom: Comparison between the structural configuration obtained at the end of the model (0 Ma) and the geological (post-thrusting) cross-section of McQuarrie and DeCelles (2001), assuming elastic (middle) and elastic-plastic (bottom) rheologies.

2003) and the medial foredeep depozone for the Tariquía Formation (Uba et al., 2006).

4.3. 14 Ma evolutionary stage

At this stage only Petaca Formation was deposited (Fig. 6d). When we stopped the model at 14 Ma, maximum sedimentary thickness of circa 4500 m was obtained for the wedge-top/foredeep depozone, ~280 km west (Figs. 6d and 11) from the area studied by Uba et al. (2005, 2006). The "saw-toothed" variation in modelled thickness registered in the western part of the profile (west of 280 km) (Figs. 6d and 11) indicates the existence of unconformities and erosion as a result of the deformation front propagation. During this time, the deformation front is at ~270 km and the modelled basin width is ~180 km. The measured and modelled sedimentary thicknesses do not show a good fit (RMS difference between measured and modelled thickness is ~60 m) (Fig. 11). The short wavelength variations of measured thicknesses could not be matched (Fig. 11). Particularly, measured thickness decreases rapidly from 100 to 0 m between ~530 and 550 km (Fig. 11). This rapid decrease in thickness could be due to erosional modification or non/low sedimentation in a forebulge or backbulge depozone (Uba et al., 2006).

We varied the input data systematically to improve the match (see Section 3.2 and Table 1). In addition, in order to estimate the sensitivity of the model to such changes and to assess the robustness of any result, we carried out a number of different tests. For example, on the same structural setting (see Table 1), we compared the sedimentary thicknesses predicted by our model considering: a) different sedimentation rates, b) different elastic thicknesses, and c) different horizontal compressive stresses. In the first case, a variation of ± 10 m in the predicted sedimentary thicknesses in the deepest sector of the basin corresponds to a change of ± 2 m/My in the sedimentation rate; such variation progressively diminishes towards the basin margin (elastic thicknesses were not changed and horizontal compressive stresses were not applied). In the second scenario, 165 m increase in the predicted sedimentary thickness is registered in the deepest sector of the basin, when we use a constant 65 km elastic thickness along the profile instead of using the elastic thickness depicted in Fig. 5a. Such increment progressively diminishes towards the basin margin (sedimentation rates were not changed and horizontal

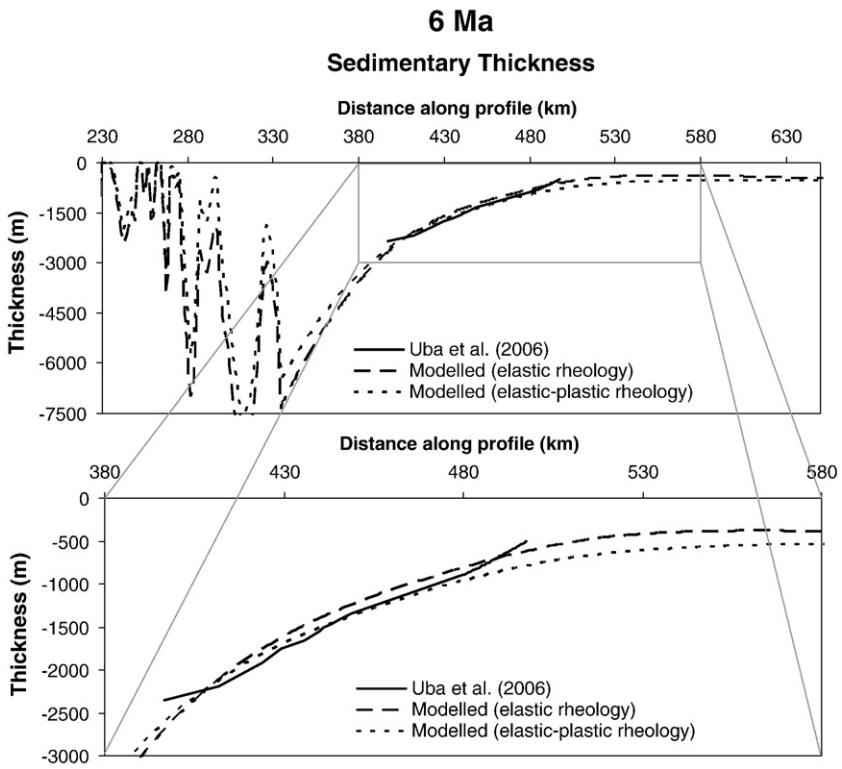

Fig. 10. Modelled vs. measured sedimentary thicknesses along the profile for the 6 Ma evolutionary stage assuming both elastic and elastic-plastic rheologies.

compressive stresses were not applied). In addition, the basin width (wavelength) also varied because the basin margin displaces 20 km to the east. Under the same conditions, when we applied a constant elastic thickness of 40 km (instead of using the elastic thicknesses depicted in Fig. 5a) a diminution of 28 m in the predicted sedimentary thicknesses was observed in the deepest sector of the basin, and the basin margin was displaced 12 km to the west. In the third case, when we used a constant 65 km elastic thickness along the profile with no

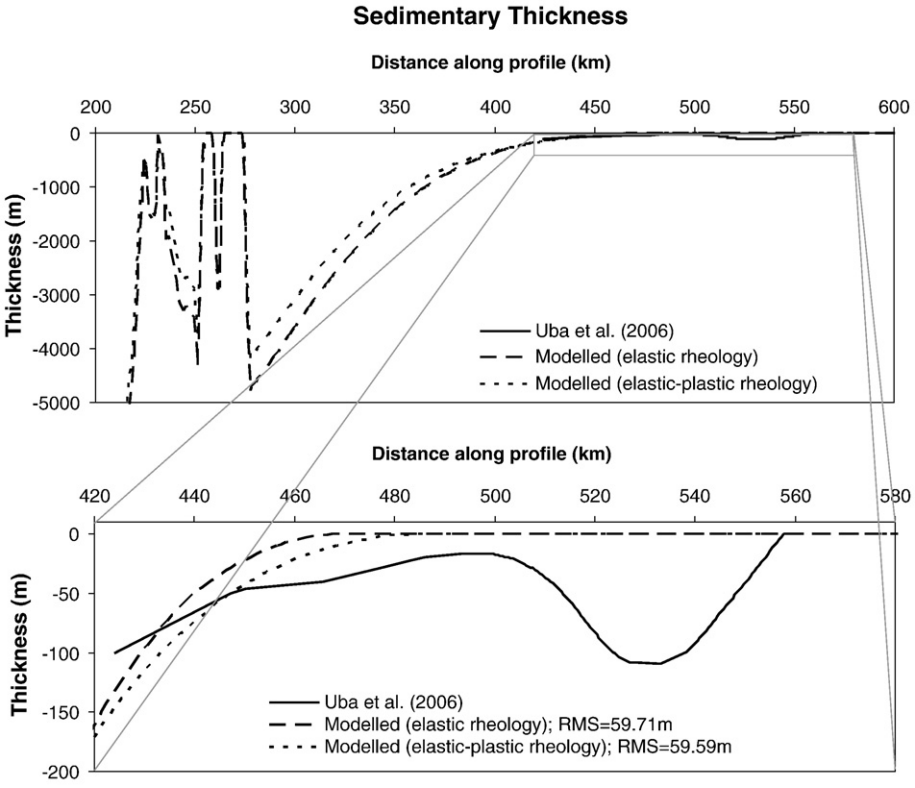

Fig. 11. Modelled vs. measured sedimentary thicknesses along the profile for the 14 Ma evolutionary stage assuming elastic rheology using the elastic thicknesses proposed by Tassara (2005, profile 5) and elastic-plastic rheology, using the geotherms before deformation proposed by Springer (1999).

change in the sedimentation rate, the application of different horizontal compressive stresses decreased the predicted sedimentary thicknesses and the basin wavelength. Furthermore, we observed that every applied unit of horizontal compressive stress (10^{12} N/m) caused 40 m decrease in thickness in the deepest part of the basin, and resulted in both 7 km eastward displacement of the basin margin and 18 km westward displacement of the backbulge depozone.

Sedimentation rate and structural settings at 14 Ma in the study area are well documented (e.g., Kley et al., 1997; McQuarrie, 2002; Uba et al., 2006, 2007, 2009). In contrast, there is no estimate for the elastic thickness along the profile at 14 Ma. In view of this shortcoming, we tested the effects of changes in the elastic thickness on the modelled sedimentary thicknesses without altering the sedimentation and structural inputs. The present elastic thickness estimates along the profile (e.g., Tassara, 2005; Tassara et al., 2006, Fig. 5a) are used as a lower constraint on the possible elastic thickness at 14 Ma. Taking into account the present ~65 km elastic thickness below the Chaco plain (e.g., Tassara, 2005; Tassara et al., 2006); we constrained the upper limit of the elastic thickness at 65 km along the profile at 14 Ma. Based on these assumptions, we used different elastic thicknesses (e.g., 65, 40, 30 to 60, 50, 40 to 60 km) to run the model. Interestingly, no acceptable fit was attained (Fig. 12a shows some examples and the corresponding RMS differences). As a result of the misfit, we considered the possible existence of total normal horizontal compressive stresses at 14 Ma.

For this model, the total normal horizontal stress represents the sum of all horizontal stress acting along the modelled profile. The total normal horizontal stress acting on Nazca–South America convergent continental margin results from the compressive force imposed by the convergence and the extensional forces related to the gravitational relaxation of the orogen (Froidevaux and Isacks, 1984; Medvedev et al., 2006). Tassara (2005) observed by flexural analysis in the Central Andes that the present-day total normal horizontal stress at the latitude of our profile is zero. This zero total normal horizontal stress suggests that the compressive forces exerted by the convergence are balanced by the horizontal extensional forces produced by the weight of the topography. Allmendinger et al. (1997) assumed this state of stress for the high Andes to calculate the horizontal compressive force resulting from the plate convergence. Based on the suggestions by Froidevaux and Isacks (1984) coupled with: a) 4 km average present altitude above sea level of the Altiplano–Eastern Cordillera, b) 2.67 kg/cm^3 density of the topographic structure, c) −0.5 kg/cm^3 density contrast between the crustal root and the mantle, and d) 35 km normal crustal thickness for the cratonic region

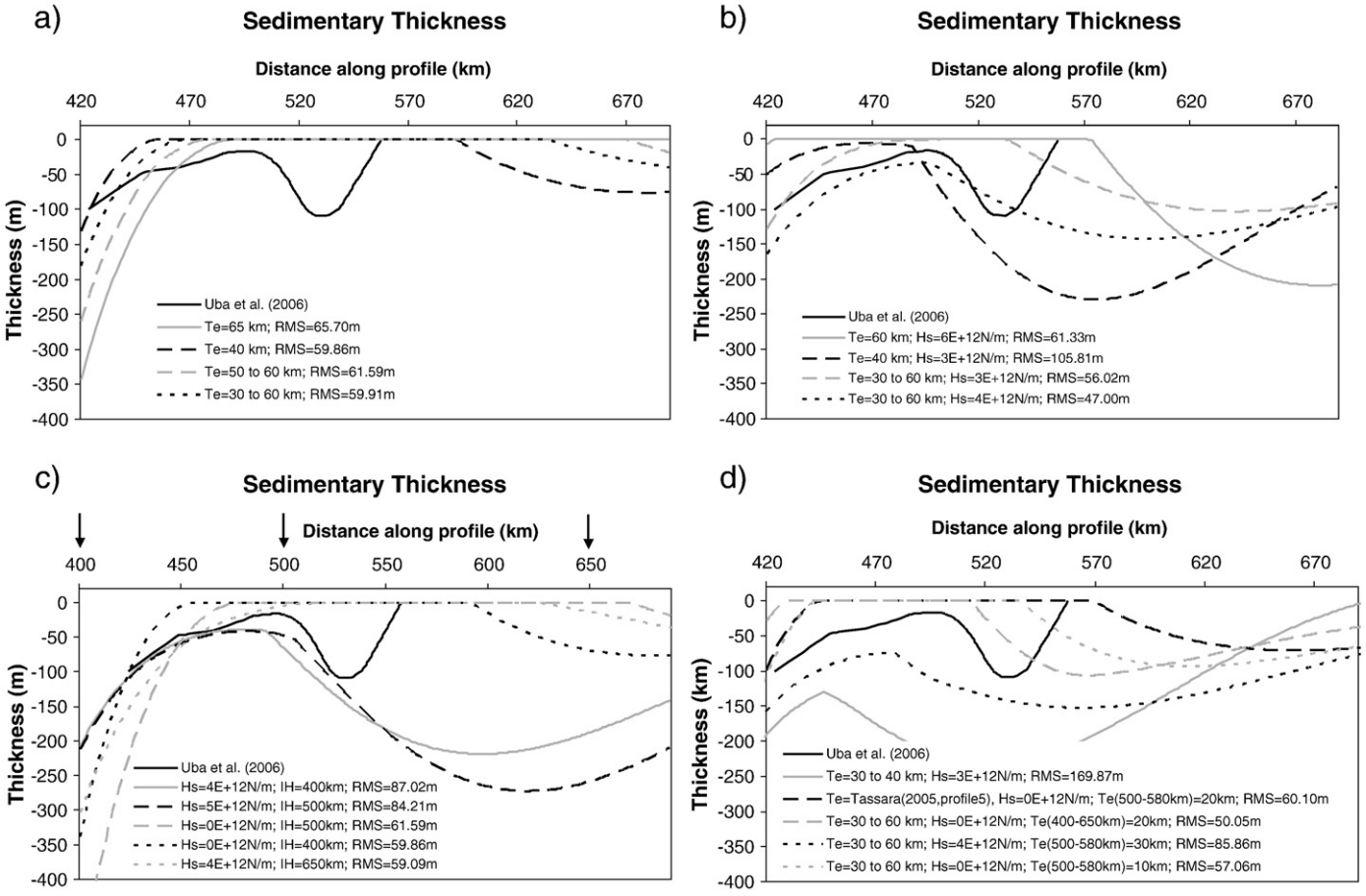

Fig. 12. Modelled vs. measured sedimentary thicknesses along the profile for the 14 Ma stage. The corresponding RMS differences are shown. a) Assuming elastic rheology, using as input constant elastic thicknesses along the profile of 65 and 40 km, using linearly increasing values of elastic thickness from 30 km in the western to 60 km in the eastern extremes of our profile and using linearly increasing values of elastic thickness from 50 km in the western to 60 km in the eastern extremes of our profile. Te: elastic thickness. b) Assuming elastic rheology, using as input diverse values of elastic thickness and applying different total normal horizontal compressive stresses. Te: elastic thickness; Hs: total normal horizontal compressive stress. c) Assuming elastic rheology, using as input linearly increasing values of elastic thickness from 30 km in the western to 60 km in the eastern extremes of our profile, applying different total normal horizontal compressive stresses, and including the Izozog High as initial topography. We assumed that at 40 Ma the Izozog High had an altitude of 500 m and was located at ~400 km, 500 km or 650 km. Hs: total normal horizontal compressive stress; IH: location of the Izozog High at 40 Ma; Black arrows: position of the maximum height of the Izozog High. d) Assuming elastic rheology, using as input the elastic thicknesses proposed by Tassara (2005, profile 5), using linearly increasing values of elastic thickness from 30 km in the western to 60 km in the eastern extremes of our profile, using linearly increasing values of elastic thickness from 30 km in the western to 40 km in the eastern extremes of our profile, applying different total normal horizontal compressive stresses and considering lower values of elastic thickness (e.g. 30, 20, 10 km) between 500 and 580 km and between 400 and 650 km. Te: elastic thickness; Hs: total normal horizontal compressive stress.

of zero altitude; we estimated the present-day normal vertical stress at 5.9×10^{12} N/m. This estimation constrains the upper boundary for the present-day prevailing horizontal plate compression, which is overtaken by the normal vertical stress. The fact that the total normal horizontal stress in the high Andes is zero does not conclude that at the lower elevation (e.g., in the Subandean Zone), it is also zero. On the contrary, it is large there (Allmendinger et al., 1997). This total normal horizontal stress would be taken up by the shortening and the deformation registered in the Subandean Zone and modelled in our profile. However, several studies suggest lower elevations of ~1.5 km, less than the half of the present altitude, for the Altiplano and Eastern Cordillera at ~15 Ma (Kennan, 2001; Lamb and Davis, 2003; Garzione et al., 2006; Barke and Lamb, 2006). In this scenario, the compressive force exerted by the convergence would not be totally balanced by the extensional force related to the gravitational relaxation of the orogen (assuming constant plate-boundary forces). In light of this, we estimate a total normal horizontal stress of 4.2×10^{12} N/m at 15 Ma. The thrusts included in the Eastern Cordillera section of our profile would absorb part of this total normal horizontal stress, however, because our model does not consist of the Altiplano, the existence of an "external" horizontal stress should be considered. The estimated 4.2×10^{12} N/m total normal horizontal stress would impose an upper limit to the "external" horizontal stress at 14 Ma. Fig. 12b shows some of the results and the corresponding RMS differences obtained applying different "external" horizontal stresses and using distinct elastic thicknesses. If we use as input the elastic thicknesses proposed by Tassara (2005) or the geotherms proposed by Springer (1999) (Fig. 5), the lithosphere obtained was too weak and did not resist any compression. After many trials, the measured and modelled sedimentary thicknesses did not show a good fit. Particularly, the rapid diminution of sedimentary thickness from 100 to 0 m between ~530 and 550 km could not be reproduced. Nevertheless, between ~420 and 530 km a reasonable fit (RMS misfit of 47.00 m) was obtained considering elastic thicknesses that linearly increase from 30 km in the western to 60 km in the eastern extremes of our profile and applying an "external" horizontal stress of 4×10^{12} N/m (Fig. 12b).

To improve the match between measured and modelled thicknesses, we introduced a new constraint in the model by the inclusion of the Izozog High as an initial topography. The Izozog High is a pre-Mesozoic structural high that runs parallel to the Andean structure (Fig. 1) (Uba et al., 2006, 2009). Fig. 12c shows some of the results and the corresponding RMS differences obtained assuming that at 40 Ma the Izozog High had an altitude of 500 m and was located at ~400 km, 500 km or 650 km. Different elastic thicknesses (including linearly increasing ones and those proposed by Tassara (2005)) and "external" horizontal stresses were used; however, no fit was obtained.

The short wavelength basement flexure necessary to reproduce the rapid diminution of sedimentary thickness from 100 to 0 m between ~530 and 550 km, could not be generated by applying in-plane compression or by considering the presence of the Izozog High. The predicted wavelength is too long, suggesting that a low value of elastic thickness should be assumed locally in this part of the basin. Fig. 12d shows some of the results and the corresponding RMS differences obtained considering distinct elastic thicknesses, applying different "external" horizontal stresses and using lower values of elastic thickness (e.g. 30, 20, 10 km) between 500 and 580 km and between 400 and 650 km. After many trials, the measured and modelled sedimentary thicknesses did not show a good fit. This persistent misfit would suggest that at ~530–550 km a significant structural element or process is missing from the model, or that erosional modification occurred in this sector of the basin. The structural setting at 14 Ma in the study area is well documented (e.g., Kley et al., 1997; McQuarrie and DeCelles, 2001; McQuarrie, 2002; McQuarrie et al., 2005: Uba et al., 2009) and does not show the existence of deformation or structural highs at ~530–550 km. Likewise, no evidences for the occurrence of other processes like thermal-induced uplift or piecemeal delamination have been reported. On the other hand, a local reduction of the sedimentation rate might be responsible for the misfit (in our model we consider spatially constant sedimentation rates; see Section 3.3). However, the rapid decrease in measured sedimentary thickness between ~530 and 550 km could also be the result of post 14 Ma erosion.

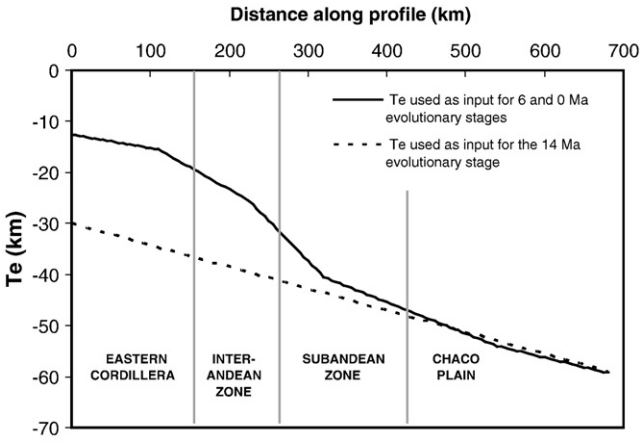

Fig. 13. Elastic thickness vs. distance along our modelled profile. Solid line: present-day estimates along ~22.6°S (Tassara, 2005, profile 5) used as input for the 6 and 0 Ma evolutionary stages. Dotted line: values used as input for the 14 Ma evolutionary stage, which linearly increase from 30 km beneath the Eastern Cordillera to 60 km beneath the Chaco plain. Note that present-day estimates beneath the Eastern Cordillera and the Interandean Zone are 18–10 km lower than the values used as input for the 14 Ma evolutionary stage. On the other hand, both sets of values are very similar beneath the Subandean Zone and the Chaco plain. Te: elastic thickness.

In spite of the persistent misfit mentioned above, the lowest RMS difference (47.00 m) was obtained using elastic thicknesses that linearly increase from 30 km in the western to 60 km in the eastern limits of our profile, coupled with an "external" horizontal stress of 4×10^{12} N/m (Fig. 12b). Such elastic thicknesses are between 18 and 10 km larger than the present-day estimations beneath the Eastern Cordillera and the Interandean Zone (Tassara, 2005, profile 5) (Fig. 13). It is important to highlight that this model predicts sedimentary thicknesses (between ~420 and 530 km), which are in agreement with measured ones (Uba et al., 2005, 2006) and supports the forebulge–backbulge depozone interpretation by Uba et al. (2006). Furthermore, our model predicts that between 14 and 6 Ma the forebulge migrated ~275 km to the east, while between 6 and 0 Ma the forebulge migrated ~35 km eastward.

5. Discussion and conclusions

Our results show that it is possible to reasonably match present-day elevation, gravity anomaly, Moho depth, elastic thicknesses, foreland sedimentary thickness, and the foreland basin configuration by applying a simple flexural modelling based on available structural information (e.g., Kley et al., 1997; McQuarrie, 2002). McQuarrie and DeCelles (2001) and McQuarrie (2002) linked the Central Andean plateau development to the creation and propagation of two major basement megathrusts sheets (10 to 15 km thick and ~200 km long) over a half-crustal-scale ramp. Interestingly, our model suggests that such basement megathrusts sheets would be more effective in reproducing the Chaco foreland basin geometry than the deep-seated basement thrusts proposed by Müller et al. (2002) (see Fig. 9). Such deep-seated thrusts probably account for the greater magnitude of shortening that Müller et al. (2002) documented. This structural configuration would create larger loads, which would generate excessive subsidence and sedimentary thickness in the Chaco basin.

In addition, our model shows a good fit between the area of maximum subsidence in the basin and the obtained area of maximum

flexural deflection. The modelled basin geometry (Fig. 6) permits the characterization of the depozones as: proximal foredeep/wedge-top depozones at 0 Ma; medial–distal foredeep depozones at 6 Ma and forebulge–backbulge depozones at 14 Ma respectively. This basin characterization is consistent with the interpretations by Uba et al. (2006) based on 2D industry seismic data, wire-line logs, and outcrop stratigraphic profiles. This modeling approach also allowed for the investigation and prediction of the spatiotemporal evolution of the foreland basin system: for example, the amount of migration of the Andean deformation front in time (e.g., 80 km between 30 and 20 Ma; 20 km between 20 and 14 Ma; 70 km between 14 and 6 Ma, 60 km between 6 and 0 Ma). Furthermore, through the model the foreland basin wavelength could be estimated (e.g., 80 km at 30 Ma, 180 km at 14 Ma, 230 km at 6 Ma, 270 km at 0 Ma).

It is worthy to note that the estimated elastic thicknesses based on elastic-plastic rheology show a very good fit with the estimates by Tassara (2005). Interestingly, the results obtained assuming different lithospheric rheologies and independent input data are remarkably coincident. Therefore, our results validate the elastic thicknesses (Tassara, 2005) and geotherms (Springer, 1999) used as input in the case of elastic and elastic-plastic rheology respectively.

A very good fit was observed between measured and modelled sedimentary thicknesses at 0 and 6 Ma when the elastic thicknesses reported by Tassara (2005) and the geotherms proposed by Springer (1999) (see Section 3.2.3) were used as input parameters. However, a good fit was not obtained between measured and modelled thicknesses at 14 Ma. The best results (lowest RMS of 47.00 m) were attained using elastic thicknesses that linearly increase from 30 km at the western to 60 km at the eastern edges of the profile (Fig. 13) coupled with an "external" horizontal stress of 4×10^{12} N/m. Nevertheless, the rapid decrease in sedimentary thickness documented between ~530 and 550 km (Fig. 12b) could not be reproduced by our model. In this sector of the basin, no signs of deformation, structural highs, thermal uplift or piecemeal delamination prior to 14 Ma have been documented (see Section 4.3). Moreover, the wavelength of such thickness variation is too short (~20 km) to have been caused by flexural effects, thus, suggesting probably the occurrence of post 14 Ma extensive erosion. However, the presence of calcretes would indicate the prevalence of non sedimentation (Uba et al., 2006). On the other hand, a local reduction of the sedimentation rate could be responsible for the thickness diminution (in our model we consider spatially constant sedimentation rates; see Section 3.3). Further work and analysis are necessary to elucidate this issue. In spite of this misfit, the long wavelength thickness distribution was satisfactorily replicated. The sedimentary thickness (between ~420 and 530 km) and the forebulge location and extension predicted by our best fit model are in agreement with those documented by Uba et al. (2005, 2006). Thus, we consider that the short wavelength misfit is not due to flexural effects that could not be reproduced by our model. The RMS misfit between modelled and measured sedimentary thicknesses between ~420 and 530 km (without considering the rapid decrease in thickness documented between ~530 and 550 km) is 20.2 m, suggesting that our best fit model can be regarded as reliable.

The elastic thicknesses used as input in our best fit model (which allowed to obtain an acceptable match between measured and modelled sedimentary thicknesses between ~420 and 530 km at 14 Ma) are approximately 100 to 50% larger than the present-day ones (Tassara, 2005; Tassara et al., 2006) beneath the Eastern Cordillera and the Interandean Zone (Fig. 13). On the other hand, both values are very similar beneath the Subandean Zone and the Chaco plain (Fig. 13). Therefore, our results suggest that a decrease in the elastic thickness beneath the Eastern Cordillera and the Interandean Zone could have occurred between 14 and 6 Ma. This suggestion is supported by Toth et al. (1996), who based on a 2D flexural modelling along 22°S with a laterally uniform rigidity elastic plate, postulated that a dramatic reduction of the elastic thickness (from 70 to 15 km) at 9–7 Ma was necessary to fit the observed stratigraphic thickness and basin geometry. Furthermore, Cardozo and Jordan (2001) used 2 and 3D flexural modelling farther south (between ~29° and 32°S) to show that at 9 Ma the elastic thickness distribution was similar to the present lithospheric strength field. They observed that 5–10 km of the lithosphere is sufficiently strong to behave as an elastic plate; however, as much as 32 km of the crust is strong enough to generate earthquakes. They concluded that such discrepancy could be the result of transient conditions, which could have made the region weak prior to 10 Ma. Toth et al. (1996) and Cardozo and Jordan (2001) conclusions thus are in agreement with the decrease in elastic thickness suggested by our modelling. However, considering the uncertainties of our results (short wavelength misfit of measured and modelled sedimentary thicknesses and possible subsequent erosion) further work is necessary to assess the significance of such reduction.

A decrease in elastic thickness indicates a reduction in strength, caused by changes in the thermal structure of the lithosphere. Using numerical modelling, Sobolev et al. (2006) and Babeyko et al. (2006) showed that one of the most significant processes occurring in the Central Andes between 20 and 15 Ma capable of causing a reduction in lithospheric strength is delamination of the lower crust and mantle lithosphere, driven by gabbro–eclogite transformation in the thickening lower crust. Lower crustal delamination adds hot asthenosphere directly in contact with the base of the crust, which might partially melt and undergo convection (Babeyko et al., 2006). The development of intracrustal convection under the plateau provides rapid heating and melting at mid-crustal level, thus, reducing the brittle strength of the uppermost crust and resulting in the large-scale eruption of ignimbrites (Babeyko et al., 2006). The most intense period of ignimbrite-forming eruptions in the Central Andes began at circa 10 Ma (Trumbull et al., 2006) in temporal coincidence with the elastic thickness reduction suggested by our modelling, which could have occurred between 14 and 6 Ma. Schurr et al. (2006) carried out local earthquake tomographic studies and interpreted a high velocity and high P-wave attenuation structure beneath the Eastern Cordillera and the eastern Puna between 23 and 24°S as detaching continental lithosphere. Furthermore, these authors suggested that a similar detachment event could have taken place during the late Miocene beneath the Altiplano. McQuarrie et al. (2005) suggested that between 18° and 20°S Cenozoic deformation within the mantle lithosphere has been focused at the Eastern Cordillera–Altiplano boundary, where continual removal or piecemeal delamination of unstable lithospheric blocks would have initiated between ~40 and 25 Ma and would continue to the present. Another postulated event in the evolution of the Central Andes contemporaneous with the elastic thickness reduction suggested here is the circa 2 km uplift of Altiplano–Puna–Eastern Cordillera (Kennan, 2001; Lamb and Davis, 2003; Garzione et al., 2006), which is proposed to be the result of mantle delamination by some authors (Garzione et al., 2006; Molnar and Garzione, 2007). We suggest that thermal weakening of the lithosphere in response to delamination could be a key process in the construction of the plateau–foreland system.

A factor not considered in our modelling, however, that can contribute to basin subsidence and/or uplift, is dynamic topography. Dynamic topography is generated by flow within the mantle. Mantle convection can create or destroy sediment accommodation space. Lithgow-Bertelloni and Gurnis (1997) demonstrated that the relative position of continents with respect to large-scale mantle downwellings causes subsidence of the Earth's surface. Subduction of cold material at converging margins induces strong down-welling flow (Lithgow-Bertelloni and Gurnis, 1997). The development of the Chaco basin is ultimately linked to the subduction of the Nazca plate under the South American plate. Interestingly, global present-day dynamic topography calculated by different authors applying mantle flow modelling (e.g., Lithgow-Bertelloni and Gurnis, 1997; Lithgow-Bertelloni and Silver, 1998; Heine et al., 2008) shows that western

South America is depressed. However, present-day dynamic topography estimates for western South America at the latitude of the Central Andes range between ~−400 and −1000 m (e.g., Lithgow-Bertelloni and Gurnis, 1997; Heine et al., 2008). Such variability reveals the lack of a widely accepted, calibrated dynamic topography model (Heine et al., 2008). Moreover, Lithgow-Bertelloni and Silver (1998) noted that mantle flow models tend to over-predict the magnitude of dynamic topography. These facts, coupled with the continental scale of published dynamic topography models, hinder a detailed evaluation of its contribution to Chaco basin subsidence. Nevertheless, both the Andean orogen and the Chaco basin have the same value of present-day dynamic topography (~−400 to −1000 m), which indicates that the whole area is depressed. No differential subsidence between the orogen and the basin due to dynamic topography can be inferred from available estimates. Furthermore, the Chaco basin presents a total stratigraphic thickness of more than 7.5 km of sedimentary rocks in its deepest part (Uba et al., 2005). Our model satisfactorily reproduced such stratigraphic thickness, considering only the accommodation space generated by lithospheric flexure. The estimated subsidence due to present-day dynamic topography is an order of magnitude lower than the measured sedimentary thickness in the Chaco basin (i.e. dynamic topography could create only ~10% of the required accommodation space). Thus, considering the limitations and simplifications of our model and the lack of a detailed and widely accepted dynamic topography model, it is difficult to evaluate the role played by dynamic topography in the evolution of the Chaco foreland basin.

In spite of the numerous limitations and simplifications mentioned above, our flexural model has shown to be a useful tool for the better understanding of the relationships between the development of the Chaco foreland basin and the spatiotemporal evolution of the Andean orogen.

Acknowledgements

This research was funded by Buenos Aires University (project UBACyT-X479 to C. Prezzi) and the German Science Foundation (Deutsche Forschungs-gemeinschaft project UB61/2-1 to C. Uba). Claudia B. Prezzi gratefully acknowledges the support of an Alexander von Humboldt Foundation Fellowship from the Alexander von Humboldt Foundation during which the major part of this work was carried out. We thank Daniel Garcia Castellanos, Brian Horton and Andrés Tassara for inspiring discussions. The suggestions of N. McQuarrie and of two anonymous reviewers greatly improved our manuscript.

References

Allmendinger, R.W., Jordan, T.E., Kay, S.M., Isacks, B.L., 1997. The evolution of the Altiplano–Puna plateau of the Central Andes. Annual Review of Earth and Planetary Sciences 25, 139–174.

Babeyko, A., Sobolev, S., Vietor, T., Oncken, O., Trumbull, R., 2006. Numerical study of weakening processes in the Central Andean Back-arc. In: Oncken, O., et al. (Ed.), The Andes, Active Subduction Orogeny. Springer, pp. 495–512 (Frontiers in Earth Sciences).

Baby, P., Hérail, G., Salinas, R., Sempere, T., 1992. Geometry and kinematic evolution of passive roof duplexes deduced from cross-section balancing: example from the foreland thrust system of the southern Bolivian Subandean Zone. Tectonics 11, 523–536.

Baby, P., Moretti, I., Guillier, B., Limachi, R., Mendez, E., Oller, J., Specht, M., 1995. Petroleum system of the northern and central Bolivian sub-Andean zone. In: Tankard, A., et al. (Eds.), Petroleum basins of South America. AAPG Memoir vol. 62. pp. 445–458.

Baby, P., Rochat, P., Mascle, G., Hérail, G., 1997. Neogene shortening contribution to crustal thickening in the back-arc of the Central Andes. Geology 25, 883–886.

Barke, R., Lamb, S., 2006. Late Cenozoic uplift of the Eastern Cordillera, Bolivian Andes. Earth and Planetary Science Letters 249, 350–367.

Barnes, J., Pelletier, J., 2006. Latitudinal variation of denudation in the evolution of the Bolivian Andes. American Journal of Science 306, 1–31.

Beaumont, C., 1981. Foreland basins. Geophysical Journal of the Royal Astronomical Society 65, 291–329.

Beck, S., Zandt, G., 2002. The nature of orogenic crust in the central Andes. Journal of Geophysical Research 107 (B10). doi:10.1029/2000JB000124.

Berggren, W.A., Kent, D.V., Swisher III, C.C., Aubry, M.-P., 1995. A revised Cenozoic geochronology and chronostratigraphy. In: Berggren, W.A., et al. (Ed.), Geochronology, Time Scales and Global Stratigraphic Correlation. (Society for Sedimentary Geology) Special Publication, No. 54. SEPM, pp. 129–212.

Burov, E.B., Diament, M., 1992. Flexure of the continental lithosphere with multilayered rheology. Geophysical Journal International 109 (2), 449–468.

Burov, E., Diament, M., 1995. The effective elastic thickness (Te) of continental lithosphere: what does it really mean? Journal of Geophysical Research 100 (3), 3905–3927.

Cardozo, N., Jordan, T., 2001. Causes of spatially variable tectonic subsidence in the Miocene Bermejo foreland basin. Argentina, Journal of Basin Research 13, 335–357.

Catuneanu, O., 2004. Retroarc foreland systems — evolution through time. Journal of African Earth Sciences 38, 225–242.

Coudert, L., Frappa, M., Viguier, C., Arias, R., 1995. Tectonic subsidence and crustal flexure in the Neogene Chaco Basin of Bolivia. Tectonophysics 243, 277–292.

DeCelles, P., Horton, B., 2003. Early to middle Tertiary foreland basin development and the history of Andean crustal shortening in Bolivia. Geological Society of America Bulletin 115 (1), 58–77.

DeCelles, P.G., Giles, K.N., 1996. Foreland basin systems. Basin Research 8, 105–123.

Dunn, J.F., Hartshorn, K.G., Hartshorn, P.W., 1995. Structural styles and hydrocarbon potential of the Subandean thrust belt of Southern Bolivia. In: Tankard, A.J., et al. (Ed.), Petroleum Basins of South America: Am. Assoc. Petrol. Geol. Mem., vol. 62, pp. 523–543.

Echavarria, L., Hernández, R., Allmendinger, R., Reynolds, J., 2003. Subandean thrust and fold belt of northwestern Argentina: geometry and timing of the Andean evolution. AAPG Bulletin 87 (6), 965–985.

Ege, H., (2004), Exhumations-und Hebungsgeschichte der zentralen Anden in Südbolivien, (21°S) durch Spaltspur-Thermochronologie an Apatit. PhD Thesis, 173 pp., Freie Universität, Berlin.

Ege, H., Sobel, E., Scheuber, E., Jacobshagen, V., 2007. Exhumation history of the southern Altiplano plateau (southern Bolivia) constrained by apatite fission track thermochronology. Tectonics 26 (1). doi:10.1029/2005TC001869.

Flemings, P.B., Jordan, T.E., 1989. A Synthetic stratigraphic model of foreland basins development. Journal of Geophysical Research 94 (4), 3851–3866.

Froidevaux, C., Isacks, B., 1984. The mechanical state of the lithosphere in the Altiplano–Puna segment of the Andes. Earth and Planetary Science Letters 71, 305–314.

Garcia-Castellanos, D., Fernández, M., Torne, M., 1997. Numerical modeling of foreland basin formation: a program relating thrusting, flexure, sediment geometry and lithosphere rheology. Computers and Geosciences 23 (9), 993–1003.

Garcia-Castellanos, D., Fernández, M., Torne, M., 2002. Modeling the evolution of the Guadalquivir foreland basin (southern Spain). Tectonics 21 (3). doi:10.1029/2001TC001339.

Gaspar-Escribano, J., Garcia Castellanos, D., 2004. Cenozoic vertical motions of the Catalan Coastal Ranges (NE Spain): the role of tectonics, isostasy, and surface transport. Tectonics 23. doi:10.1029/2003TC001511.

Garzione, C., Molnar, P., Libarkin, J., MacFadden, B., 2006. Rapid late Miocene rise of the Bolivian Altiplano: evidence for removal of mantle lithosphere. Earth and Planetary Science Letters 241, 543–556.

Giese, P., Scheuber, E., Schilling, F., Schmitz, M., Wigger, P., 1999. Crustal thickening processes in the Central Andes and the different natures of the Moho-discontinuity. Journal of South American Earth Sciences 12, 201–220.

Gómez, E., Jordan, T., Allmendinger, R., Cardozo, N., 2005. Development of the Colombian foreland-basin system as a consequence of diachronous exhumation of the northern Andes. GSA Bulletin 117 (9–10), 1272–1292.

Götze, H.-J., Kirchner, A., 1997. Interpretation of gravity and geoid in the Central Andes between 20° and 29°S. Journal of South American Earth Sciences 10 (2), 179–188.

Götze, H.J., Lahmeyer, B., Schmidt, S., Strunk, S., Araneda, M., 1990. Central Andes Gravity Data Base. Eos 71 (16), 401–407.

Gubbels, T.L., Isacks, B.L., Farrar, E., 1993. High-level surface, plateau uplift, and foreland development, Bolivian central Andes. Geology 21, 695–698.

Haq, B., Hardenbol, J., Vail, P., 1987. Chronology of fluctuating sea-levels since the Triassic. Science 235, 1156–1167.

Heine, C., Müller, R., Steinberger, B., Torsvik, T., 2008. Subsidence in intracontinental basins due to dynamic topography. Physics of the Earth and Planetary Interiors 171 (1–4), 252–264. doi:10.1016/j.pepi.2008.05.008.

Horton, B.K., 1998. Sediment accumulation on top of the Andean orogenic wedge: Oligocene to late Miocene basins of the Eastern Cordillera, southern Bolivia. Geological Society of America Bulletin 110 (9), 1174–1192.

Horton, B.K., 2005. Revised deformation history of the central Andes: inferences from Cenozoic foredeep and intermontane basins of the Eastern Cordillera, Bolivia. Tectonics 24. doi:10.1029/2003TC001619.

Horton, B.K., DeCelles, P.G., 1997. The modern foreland basin system adjacent to the Central Andes. Geology 25, 895–898.

Hulka, C., 2005. Sedimentary and tectonic evolution of the Cenozoic Chaco foreland basin, southern Bolivia. PhD Thesis, Freie Universität Berlin, Berlin.

Husson, L., Sempere, T.h., 2003. Thickening the Altiplano crust by gravity-driven crustal channel-flow. Geophysical Research Letters 30 (5), 1243–1247.

Jordan, T., 1981. Thrust loads and foreland basin evolution, Cretaceous, western United States. American Association of Petroleum Geologists Bulletin 65, 2506–2520.

Jordan, T.E., Flemings, P.B., 1991. Large-scale stratigraphic architecture, eustatic variation, and unsteady tectonism: a theoretical evaluation. Journal of Geophysical Research 96, 6681–6699.

Kennan, L., 2001. Large-scale geomorphology of the Andes: interrelationships of tectonics, magmatism and climate. In: Summerfield, M.A. (Ed.), Geomorphology and Global Tectonics. Wiley, p. 18.

Kley, J., 1996. Transition from basement-involved to thin-skinned thrusting in the Cordillera Oriental of southern Bolivia. Tectonics 15 (4), 763–775.
Kley, J., Gangui, A., Krüger, D., 1996. Basement-involved blind thrusting in the Eastern Cordillera, southern Bolivia: evidence from cross-sectional balancing, gravimetric and magnetotelluric data. Tectonophysics 259 (13), 171–184.
Kley, J., Monaldi, C.R., Salfity, J.A., 1999. Along strike segmentation of the Andean foreland: causes and consequences. Tectonophysics 301, 75–94.
Kley, J., Müller, J., Tawackoli, S., Jacobshagen, V., Manutsoglu, E., 1997. Pre-Andean and Andean-age deformation in the Eastern Cordillera of S Bolivia. Journal of South American Earth Sciences 10, 1–19.
Lamb, S., Davis, P., 2003. Cenozoic climate change as a possible cause for the rise of the Andes. Nature 425, 792-297.
Lithgow-Bertelloni, C., Gurnis, M., 1997. Cenozoic subsidence and uplift of continents from time-varying dynamic topography. Geology 25 (8), 735–738.
Lithgow-Bertelloni, C., Silver, P.G., 1998. Dynamic topography, plate driving forces and the African superswell. Nature 395, 269–272.
Lynch, H., Morgan, P., 1987. The tensile strength of the lithosphere and the localization of extension. In: Coward, M.P., et al. (Ed.), Continental Extension Tectonics: Geological Society Special Publication, vol. 28, pp. 53–65.
Lyon-Caen, H., Molnar, P., Suarez, G., 1985. Gravity anomalies and flexure of the Brazilian shield beneath the Bolivian Andes. Earth and Planetary Science Letters 75, 81–92.
Marshall, L., Sempere, T., 1991. The Eocene to Pleistocene vertebrates of Bolivia and their stratigraphic context: a review. In: Suárez-Soruco, R. (Ed.), Fósiles y Facies de Bolivia. Revista Técnica de YPBF, 12, pp. 631–652. Santa Cruz, Bolivia.
McQuarrie, N., 2002. Building a high plateau: the kinematic history of the central Andean fold–thrust belt, Bolivia. Geological Society of America Bulletin 114, 950–963.
McQuarrie, N., DeCelles, P., 2001. Geometry and structural evolution of the central Andean backthrust belt. Bolivia, Tectonics 20 (5), 669–692.
McQuarrie, N., Horton, B., Zandt, G., Beck, S., DeCelles, P., 2005. Lithospheric evolution of the Andean fold–thrust belt, Bolivia, and the origin of the central Andean plateau. Tectonophysics 399, 15–37.
Medvedev, S., Podladchikov, Y., Handy, M.R., Scheuber, E., 2006. Controls on the deformation of the Central and Southern Andes (10–35°S): insight from thin-sheet numerical modelling. In: Oncken, O., et al. (Ed.), The Andes, Active Subduction Orogeny. Frontiers in Earth Sciences. Springer, pp. 475–494.
Molnar, P., Garzione, C., 2007. Bounds on the viscosity coefficient of continental lithosphere from removal of mantle lithosphere beneath the Altiplano and Eastern Cordillera. Tectonics 26. doi:10.1029/2006TC001964.
Moretti, I., Baby, P., Mendez, E., Zubieta, D., 1996. Hydrocarbon generation in relation to thrusting in the Subandean Zone from 18° to 22°S, South Bolivia. Petroleum Geoscience 2, 17–28.
Müller, J., Kley, J., Jacobshagen, V., 2002. Structure and Cenozoic kinematics of the Eastern Cordillera, southern Bolivia (21°S). Tectonics 21 (5). doi:10.1029/2001TC001340.
Oller, J., 1986. Consideraciones generales sobre la geologia y estratigrafia de la Faja Subandina norte, MSc Thesis Universite Mayor de San Andres, La Paz.
Prezzi, C., Götze, H.-J., Schmidt, S., in press. The Central Andes lithospheric structure from 3D gravity modelling. In: Salfity, J., Marquillas, R. (Eds.), Cenozoic Geology of the Central Andes of Argentina.
Roddaz, M., Baby, P., Brusset, S., Hermoza, W., Darrozes, J.M., 2005. Forebulge dynamics and environmental control in Western Amazonia: the case study of the Arch of Iquitos (Peru). Tectonophysics 399, 87–108.
Schurr, B., Rietbrock, A., Asch, G., Kind, R., Oncken, O., 2006. Evidence for lithospheric detachment in the central Andes from local earthquake tomography. Tectonophysics 415, 203–223.
Sempere, T., Hérail, G., Oller, J., Bonhomme, M.G., 1990. Late Oligocene–Early Miocene major tectonic crisis and related basins in Bolivia. Geology 18, 946–949.
Sobolev, S., Babeyko, A., Koulakov, I., Oncken, O., 2006. Mechanism of the Andean Orogeny: Insight from numerical modeling. In: Oncken, O., et al. (Ed.), The Andes, Active Subduction Orogeny. Frontiers in Earth Sciences. Springer, pp. 513–535.
Springer, M., 1999. Interpretation of heat-flow density in the Central Andes. Tectonophysics 306, 377–395.
Stewart, J., Watts, A., 1997. Gravity anomalies and spatial variations of flexural rigidity at mountain ranges. Journal of Geophysical Research 102 (B3), 5327–5352.
Talwani, M., Worzel, J., Landisman, M., 1959. Rapid gravity computations for two-dimensional bodies with application to the Mendocino submarine fracture zone. Journal of Geophysical Research 64, 49–59.
Tassara, A., 2005. Interaction between the Nazca and South American plates and formation of the Altiplano–Puna plateau: review of a flexural analysis along the Andean margin (15°–34°S). Tectonophysics 399, 39–57.
Tassara, A., Swain, C., Hackney, R., Kirby, J., 2006. Elastic thickness structure of South America estimated using wavelets and satellite-derived gravity data. Earth and Planetary Science Letters 253, 17–36.
Toth, J., Kusznir, N., Flint, S., 1996. A flexural isostatic model of lithosphere shortening and foreland basin formation: application to the Eastern Cordillera and Subandean Belt of NW Argentina. Tectonics 15 (1), 213–223.
Turcotte, D., Schubert, G., 2002. Geodynamics, 2nd ed. Cambridge Univ. Press, New York. 456 pp.
Trumbull, R., Riller, U., Oncken, O., Scheuber, E., Munier, K., Hongn, F., 2006. The time–space distribution of Cenozoic volcanism in the South-Central Andes: a new data compilation and some tectonic implications. In: Oncken, O., et al. (Ed.), The Andes, Active Subduction Orogeny. Frontiers in Earth Sciences. Springer, pp. 29–44.
Uba, C.E., Heubeck, C., Hulka, C., 2005. Facies analysis and basin architecture of the Neogene Subandean synorogenic wedge, southern Bolivia. Sedimentary Geology 180, 91–123.
Uba, C.E., Heubeck, C., Hulka, C., 2006. Evolution of the late Cenozoic Chaco foreland basin, Southern Bolivia. Basin Research 18, 145–170.
Uba, C.E., Strecker, M.R., Schmitt, A.K., 2007. Increased sediment accumulation rates and climatic forcing in the central Andes during the late Miocene. Geology 35, 979–982.
Uba, C.E., Kley, J., Strecker, M., Schmitt, A., 2009. Unsteady evolution of the Bolivian Subandean thrust belt: the role of enhanced erosion and clastic wedge progradation. Earth and Planetary Science Letters 281(3), 134–146.
Ussami, N., Shiraiwa, S., Landim Dominguez, J., 1999. Basement reactivation in a sub-Andean foreland flexural bulge The Pantanal wetland, SW Brazil. Tectonics 18 (1), 25–39.
Vening-Meinesz, F.A., 1941. Gravity over Hawaiian archipelago and over Madeira area. Proceedings of the Netherlands Acad. Wetensch. 44, 1–12.
Watts, A., 2001. Isostasy and Flexure of the Lithosphere. Cambridge University Press, Cambridge, U.K. 458 pp.
Watts, A., Lamb, S., Fairhead, J., Dewey, J., 1995. Lithospheric flexure and bending of the Central Andes. Earth and Planetary Science Letters 134, 9–21.
Yang, Y., Liu, M., Stein, S., 2003. A 3-D geodynamic model of lateral crustal flow during Andean mountain building. Geophysical Research Letters 30 (21). doi:10.1029/2003GL018308.
Yuan, X., Sobolev, S., Kind, R., 2002. Moho topography in the central Andes and its geodynamic implications. Earth and Planetary Sciences Letters 199, 389–402.
Zeyen, H., Negredo, A., Fernández, M., 1996. Extension with lateral accommodation—"active" vs. "passive" rifting. Tectonophysics 266 (1–4), 121–137.